Ref. Ares(2025)5141969 - 27/06/2025

Funded by the European Union

Horizon Europe programme, grant agreement No. 101096068

# RETROFIT SOLUTIONS TO ACHIEVE 55% GHG REDUCTION BY 2030

## Report on hydrodynamic optimization of ships with WASP & relevant response surfaces

| |
|---|
| WP 2 – Hydrodynamic design optimization |
| Task 2.2 – Hydrodynamic optimization of ships with WASP |
| D2.2 – Report on hydrodynamic optimization of ships with WASP & relevant response surfaces |
| Partners involved: FSYS, SFWD |
| Authors: H. Renzsch, F. Thies, D. Ntouras, K. Kostalas, R. D’Souza, V. Zagkas |

## Project details

| | |
|---|---|
| **Project Title** | RETROFIT SOLUTIONS TO ACHIEVE 55% GHG REDUCTION BY 2030 |
| **Project Type** | Innovation Action |
| **Project Acronym** | RETROFIT55 |
| **Grant Agreement No.** | 101096068 |
| **Duration** | 36 M |
| **Project Start Date** | 01/01/2023 |

## Deliverable information

| | |
|---|---|
| **Status**<br>(F: final; D: draft; RD: revised draft) | F |
| **Planned delivery date** | 31/12/2024 |
| **Actual delivery date** | 23/06/2025 |
| • **Dissemination level:** PU – Public, fully open, e.g. web (Deliverables flagged as public will be automatically published in CORDIS project's page)<br>• SEN – Sensitive, limited under the conditions of the Grant Agreement<br>• Classified R-UE/EU-R – EU RESTRICTED under the Commission Decision No2015/444<br>• Classified C-UE/EU-C – EU CONFIDENTIAL under the Commission Decision No2015/444<br>Classified S-UE/EU-S – EU SECRET under the Commission Decision No2015/444 | PU |
| **Type: Report, Website, Other, Ethics** | Report |

## Document history

| Version | Date | Created/Amended by | Changes |
|---|---|---|---|
| 01 | 13/02/2025 | Dimitris Ntouras, (SFD) | Report structure |
| 02 | 12/03/2025 | Reuben D'Souza (SFD) | Draft version for review |
| 03 | 16/04/2025 | Reuben D'Souza (SFD) | First revision incorporating technical reviewers comments |
| 04 | 29/05/2025 | Dimitris Ntouras, Reuben D'Souza (SFD) Hannes Renzsch (FSYS) | Second revision incorporating technical reviewers comments |
| 05 | 18/06/2025 | Hannes Renzsch (FSYS) | Pre-final version |
| Final | 23/06/2025 | Hannes Renzsch (FSYS) | Minor revisions Final version |

## Quality check review

| Reviewer (s) | Main changes / Actions |
|---|---|
| Emanuele Spinosa and Riccardo Broglia (CNR) | Technical review |
| Cecilia Leotardi (CNR) | Technical and editorial review |
| Cecilia Leotardi and Alessandro Iafrati (CNR) | Final review of contents and submission to EC. |

## Table of Contents

List of figures ....................5
List of tables....................6
List of acronyms....................7
Executive Summary....................8
1 Introduction....................9
2 Scope, objective, and structure of the report....................10
2.1 Scope and objectives....................10
2.2 Structure....................10
3 Geometry description of the bulk carrier vessel....................12
4 Hydrodynamic design considerations of ships in heel conditions....................14
5 Hydrodynamic design considerations of ships in drift conditions....................17
5.1 Systematic analysis of resistance, side force and yaw moment as function of drift....................17
5.1.1 Surrogate modelling of drift-induced forces and moments....................18
5.2 Effect of ESDs in drift conditions....................20
5.3 Analysis of influence of speed, draught, trim and drift on the nominal wake field in presence of an existing pre-swirl duct....................24
5.3.2 CFD-Simulations and DoE....................25
5.3.3 Evaluation of the nominal wake field....................25
6 Hydrodynamic design optimization of ship with WASP....................27
6.1 Scope of optimisation....................27
6.1.1 Forebody....................27
6.1.2 Deadwood....................28
6.1.3 Design of experiment....................28
6.2 Results....................28
7 Open water rudder tests....................35
8 Closing remarks....................38
References....................39

## List of figures

Figure 1: Ship experiencing a drift and heel angle under the presence of wind propulsion engine. . 9
Figure 2: Comparison between the 3D model and the drawings of M/V Kastor. ........................... 13
Figure 3: Resistance and attitude results for MV Kastor for various heel angles for $T_{sc}$=14.45m and V=14.0kn. ........................................................................................................ 14
Figure 4: Contour of the hydrodynamic on the bow of the hull for $T_{sc}$=14.45m and V=14.0kn........ 15
Figure 5: Pressure contour on the surface of the rudder for $T_{sc}$=14.45m and V=14.0kn. .............. 15
Figure 6: Free surface elevation for $T_{sc}$=14.45m and V=14.0kn. ................................................ 15
Figure 7: Relative velocity at propeller plane for $T_{sc}$=14.45m and V=14.0kn................................ 16
Figure 8: Forces and longitudinal center of effort (xCE), relative to aft perpendicular, as function of drift angle. ........................................................................................................ 17
Figure 9: Vorticity-X on cutting plane 50m in front of aft perpendicular at 6° drift. ......................... 18
Figure 10: Visualization of resampled surrogate model. ............................................................ 20
Figure 11: Duct with two half-rings fitted on the bulk carrier M/V Kastor. ..................................... 21
Figure 12: Free surface elevation for different drift angles and for $T_{sc}$=14.45m and V=13.5kn....... 21
Figure 13: Effect of ESD for different drift conditions and for Tsc=14.45m and V=13.5kn............. 22
Figure 14: Contour of the velocity deficit at the propeller plane disk influenced by the presence of a duct with two half-rings in drift conditions. ........................................................................ 23
Figure 15: Flow visualization of vortex system created in case of β=6°. ....................................... 24
Figure 16: Pre-swirl duct fitted to Kastor. ................................................................................ 24
Figure 17: Correlations between operating conditions and wake field. ........................................ 25
Figure 18: Wake field at different yaw angles. .......................................................................... 26
Figure 19: Morphing region for stem modification. .................................................................... 27
Figure 20: Investigated parameter range for stem modification. ................................................. 28
Figure 21: Deadwood extensions investigated. ......................................................................... 28
Figure 22: Residual resistance at 0, 3 and 6 deg of drift, relative to the baseline values. .............. 29
Figure 23: Added resistance due to drift. .................................................................................. 29
Figure 24: Side force generated by the drifting hulls. ................................................................. 30
Figure 25: Wave patterns of the baseline, des0007 and des0014 at 0, 3 and 6 degrees of drift. ... 30
Figure 26: Pressure distribution (dynamic) at the bow of the baseline, des0007 and des0014 at 0, 3 and 6 degrees of drift. ........................................................................................................ 31
Figure 27: Residual resistance (a) and side force (b) of the variants with a deadwood relative to the baseline values. ........................................................................................................ 32
Figure 28: TKE at deadwood at 3° drift (left to right: baseline, increasing extension). .................. 32
Figure 29: Polar plots of the required propulsion power from the propeller relative to the required power of the baseline hull. ........................................................................................... 33
Figure 30: Polar plots of the required propulsion power from the propeller relative to the required power of the baseline hull. ........................................................................................... 34
Figure 31: Computational setup for open water rudder tests. ...................................................... 35
Figure 32: Results of open water rudder tests. Lift (CL) and drag (CD) coefficient for Re=25 million. ........................................................................................................ 36
Figure 33: Axial velocity contours on symmetry plane. ............................................................... 36
Figure 34: Flow visualization of open water rudder tests. Streamtraces and pressure contours on the surface of the rudder. ........................................................................................................ 37

## List of tables

Table 1: Bulk carrier vessel's main particulars. 12
Table 2: Bulk carrier engine’s main particulars. 12
Table 3: Bulk carrier propeller's main particulars. 12
Table 4: Hydrostatic data comparison between the modeled *M/V Kastor* and as-built hull. 13
Table 5: Parameter space for Sobols and re-sampling. 19
Table 6: Parameter range for evaluation of ESD. 25

## List of acronyms

| | |
|---|---|
| AoA | Angle of Attack |
| CFD | Computational Fluid Dynamics |
| DoE | Design of Experiments |
| DSS | Decision Support System |
| ESD | Energy-Saving Devices |
| GHG | GreenHouse Gas |
| Re | Reynolds Number |
| TWA | True Wind Angle |
| TWS | True Wind Speed |
| TKE | Turbulent Kinetic Energy |
| WASP | Wind Assisted Ship Propulsion |

## Executive Summary

This report details the efforts undertaken in task T2.2 regarding the hydrodynamic optimization of ships equipped with Wind Assisted Ship Propulsion (WASP). The RETROFIT55 project aims to develop a Decision Support System (DSS) that enables the integration of diverse retrofitting solutions, achieving a 35% reduction in GHG emissions compared to original technologies. Moreover, the project combines established technologies (ship electrification, hydrodynamic design optimization, and operational optimization) with two emerging technologies (wind-assisted ship propulsion and an innovative air lubrication system).

The objective of the report is to explore the hydrodynamic aspects of the ships equipped with WASP. To this end, a bulk carrier ship has been selected as case study vessel and an assessment of its hydrodynamic behavior when sailing under induced heel and leeway angles has been carried out. The focus has been on the effectiveness of energy saving devices under these conditions. All studies have been carried out using CFD solvers.

Firstly, the report investigates the effect of heeling. In these types of ships, small angles of heel are expected and their impact on hydrodynamic performance is negligible. Thereafter, the impact of drift on ships resistance is explored. A notable increase has been found, especially for angles greater than 3°. Although the impact of the ESDs is negligible on the hydrodynamic efficiency of the hull, their positive effect on propeller efficiency is expected to be mitigated.

Moreover, in the present report a detailed analysis on the impact of speed, draught, trim and drift with and without ESD is included, to provide the necessary response surfaces to the DSS. Lastly, an optimization study has been carried out where modifications on the deadwood and stem regions are considered.

# 1 Introduction

Evaluating alternatives to reduce GHG emissions[1] in order to reach net zero emissions is imperative and energy efficiency measures that are largely under-utilized must be examined. RETROFIT55, an EU funded project, aims to develop decarbonization solutions and green technologies which can be used by ship-owners to minimize fuel consumption and Greenhouse Gas (GHG) emissions. The use of ESDs as short-term emission reduction measures is considered a key factor in the energy transition of commercial shipping. Wind assisted propulsion standing apart among available technologies, promises fuel savings that in combination with other energy saving technologies may set the foundation for transition to net zero emissions. The adoption of technologies such as WASP devices to vessels necessitates a reassessment of resistance components and hydrodynamic optimization to mitigate these abrupt changes. The present study has focused on the implementation of design alternatives, such as the optimization of the geometry in the fore and aft regions of the hull, and the evaluation of existing variations of energy saving devices in the aft part of the hull and in the propeller itself. To achieve that, the effects of these implementations will be quantified for the vessels under study and will provide a valuable input for the selection of ESDs and the consideration of the heel and leeway angles respectively.

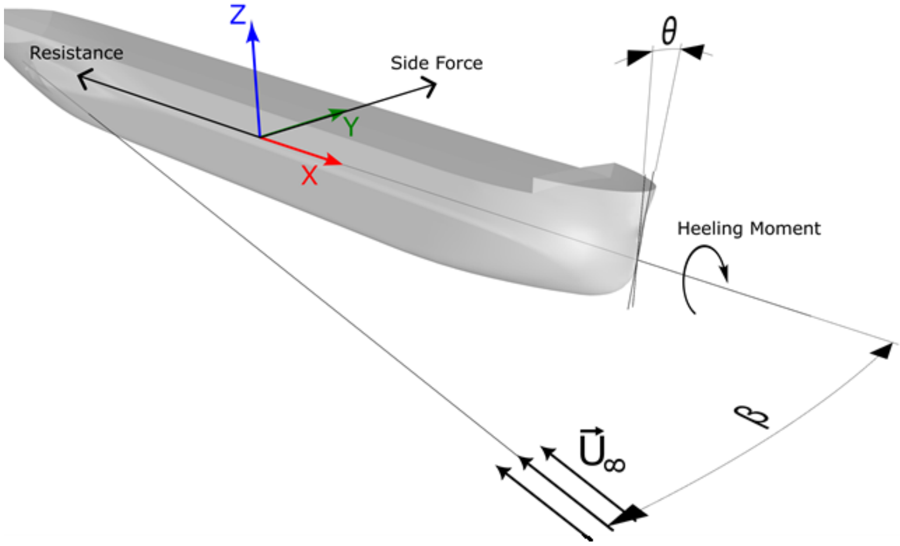


Figure 1: Ship experiencing a drift and heel angle under the presence of wind propulsion engine.

The principles of basic ship dynamics demonstrate that the lateral force exerted on the vessel, arising from the wind propulsor, generates a yawing moment that results in leeward drift. This drift manifests as an angle between the vessel's heading and its actual path, concurrently changing the pressure distribution around the hull. Furthermore, a heeling moment is created due to the wind pressure on the sails. An example of ship sailing under heel and drift angles is given in Figure 1. The aim is to thoroughly investigate these phenomena, evaluate their consequences, and determine their significance.

[1] https://climate.ec.europa.eu/eu-action/transport/reducing-emissions-shipping-sector_en

# 2 Scope, objective, and structure of the report

## 2.1 Scope and objectives

The objective of this report is to present a comprehensive analysis of the methodology and solutions proposed for the hydrodynamic optimization of ships with WASP devices installed, in alignment with the scope of the RETROFIT55 project.

The current report assesses the hydrodynamic performance of one case study vessel and the effects on its performance after the introduction of a WASP device. It investigates the changes in hydrodynamic resistance and the effects of energy saving devices on the propulsion efficiency when the vessel operates under a constant drift angle. For this analysis, a bulk carrier was selected due to its unique attributes as a cargo ship with a high block coefficient and low operational speed.

The presented results are produced by a joint effort between two partners of the RETROFITT55's consortium. The methodologies for each optimization case are detailed in this report, including justifications for simplifications and assumptions. The computational tools used are mentioned and a discussion of the results and retrofitting solution principles has been listed.

The effects of each retrofitting technology and the results of this study will be incorporated as input to WP1 which primarily demonstrates the development of the DSS.

## 2.2 Structure

The report meticulously documents the consortium's endeavors to create retrofitting solutions that optimize the ship's hydrodynamic design after having incorporated a WASP installation. It illustrates how these efforts align with the respective goals of the RETROFIT55 project, as defined by the Grant Agreement.

The structure of the report is the following:

- The introduction addresses a brief overview of the RETROFIT55 project and the goals of hydrodynamic optimization after the introduction of a wind assisted propulsor device.
- The scope, objective, and structure chapter of the report addresses the explanation on how hydrodynamic optimization aligns with the RETROFIT55 objectives, the framework and the goals of the studies presented, and the overall description of the report structure.
- The geometry description chapter presents the principal characteristics of the case study vessel along with a description of the operational data used as input in the hydrodynamic optimization process. Furthermore, it provides a comparison of the 3D-CAD models generated with the actual hydrostatic data.
- Hydrodynamic design considerations of ships in heel conditions chapters includes a CFD study conducted for the bulk carrier vessel when a heel angle is introduced due to external forcing.
- Hydrodynamic design considerations of ships in drift conditions chapter is dedicated to the examinations of the hydrodynamic effects of drift in case of a bulk carrier vessel. The section includes three studies that assess the behaviour of the vessel in drift conditions, with and without ESDs as well as correlations for the influence of speed, draught, trim and drift
- Hydrodynamic design optimization of ship with WASP: An optimization study takes place that aims to improve the hydrodynamic performance of the vessel by applying modification at the stem and the deadwood regions.

- Open water rudder tests: A hydrodynamic assessment of the performance of the rudder in full scale is presented for $Re=3.5e^7$ and a range of angle of attacks (AoA).

# 3 Geometry description of the bulk carrier vessel

As reference geometry a Kamsarmax-size bulk carrier vessel is selected, owned by Laskaridis Shipping Co. The particulars of vessel, engine and propeller can be respectively in Table 1, Table 2, and Table 3. All considerations made in the following sections are based on the geometry of this vessel.

Table 1: Bulk carrier vessel's main particulars.

| | |
|---|---|
| Ship Name: | M/V Kastor |
| Ship Type: | BULK CARRIER |
| Year of Build: | 2020 |
| LPP (m): | 225.5 |
| Breadth (MLD) *(m)*: | 32.20 |
| Depth (MLD) *(m)*: | 20.05 |
| Scantling Draft *(m)*: | 14.45 |
| Extreme Draft Displ. *(t)*: | 94796.2 |
| Block Coefficient (CB): | 0.8772 |
| Lightweight *(t)*: | 13800.1 |
| IMO No. | 9843405 |
| Scantling Draft *(m)*: | 14.45 |
| Extreme Draft Displ. *(t)*: | 94796.2 |

Table 2: Bulk carrier engine’s main particulars.

| | | |
|---|---|---|
| *M.C.R* | 9930 kW | 90.4 RPM |
| *N.C.R* | 7110 kW | 80.9 RPM |

Table 3: Bulk carrier propeller's main particulars.

| | |
|---|---|
| Type: | FPP |
| Diameter *(m):* | 6.95 |
| Number of Blades: | 5 |
| P/D at 0.7R: | 0.7719 |
| Mean Pitch (*mm*): | 5258.39 |
| Expanded Area Ratio | 0.52 |
| Chord Length at 0.6R (*mm*) | 2085.0 |

SFD has developed the 3D CAD model from the structural drawings provided by Laskaridis. A comparison between the CAD model and the original drawings can be found in Figure 2.

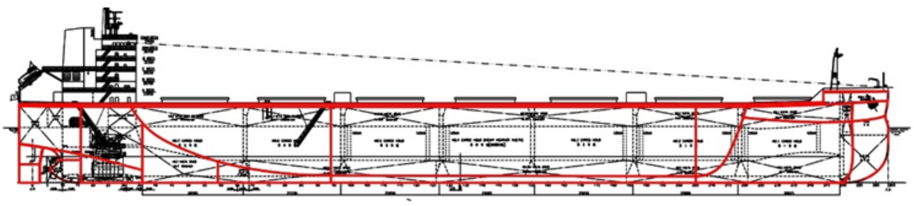

Side view comparison.

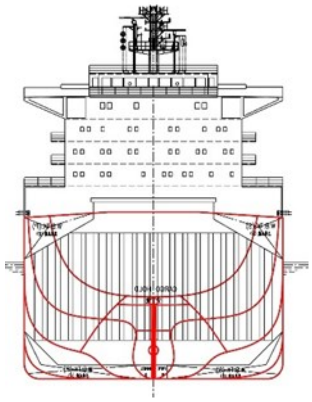

Mid-ship section comparison.

Figure 2: Comparison between the 3D model and the drawings of M/V Kastor.

In order to verify that the generated CAD model follows the actual geometry, the hydrostatic data for the 3D model and the actual ship are presented and compared in Table 4. In all cases, the differences are well below 1% for both displacement and LCB.

Table 4: Hydrostatic data comparison between the modeled *M/V Kastor* and as-built hull.

| | 3D-CAD hull particulars | | Ship particulars (from stability booklet) | | Comparison | |
|---|---|---|---|---|---|---|
| Draught | Displacement. | LCB | Displacement. | LCB | Displacement. | LCB |
| (m) | (t) | (m) | (t) | (m) | (%) | (%) |
| 3 | 17,326 | 120.058 | 17,464 | 120.148 | -0.79% | -0.07% |
| 5 | 29,807 | 119.414 | 29,962 | 119.531 | -0.52% | -0.10% |
| 7 | 42,667 | 118.679 | 42,870 | 118.795 | -0.47% | -0.10% |
| 9 | 56,065 | 117.473 | 56,258 | 117.711 | -0.34% | -0.20% |
| 10 | 62,941 | 116.849 | 63,162 | 117.021 | -0.35% | -0.15% |
| 12 | 77,011 | 115.368 | 77,289 | 115.589 | -0.36% | -0.19% |
| 14.45 | 94,516 | 113.967 | 94,796 | 114.225 | -0.30% | -0.23% |

# 4 Hydrodynamic design considerations of ships in heel conditions

This section investigates the effect of heel angle on the performance of the vessel. SFD has conducted resistance simulations for five different heel angles between 1° and 5°. CFD simulations have been carried out at full scale using the software CADENCE/FineMarine v11.2. The numerical setup follows the one presented in the deliverable D2.1 of the RETROFIT55 project. Two degrees of freedom for the vessel have been left unconstrained: heave and pitch.

In Figure 3, the results of the study are presented for heel angles between zero and five degrees for scantling draught conditions $T_{sc}$=14.45 m and ship speed V=14.0kn.

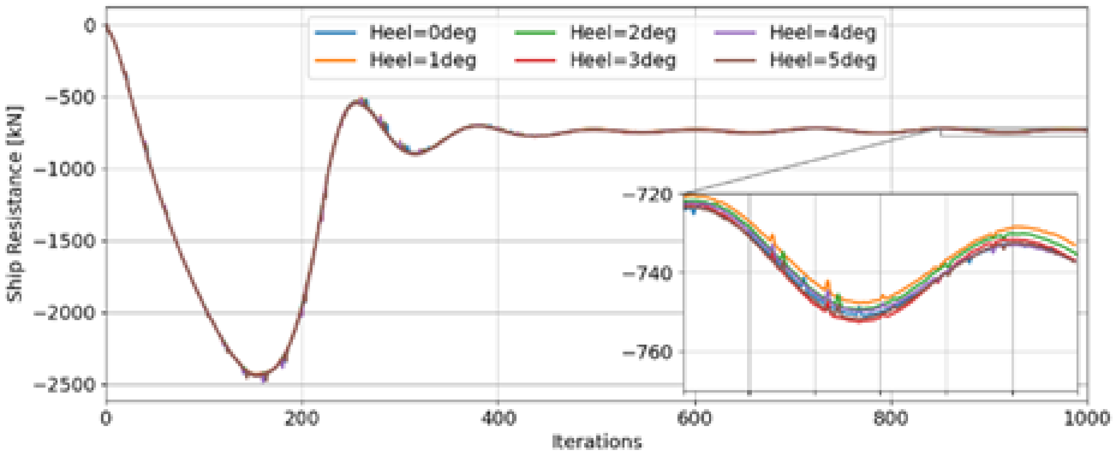


Resistance force

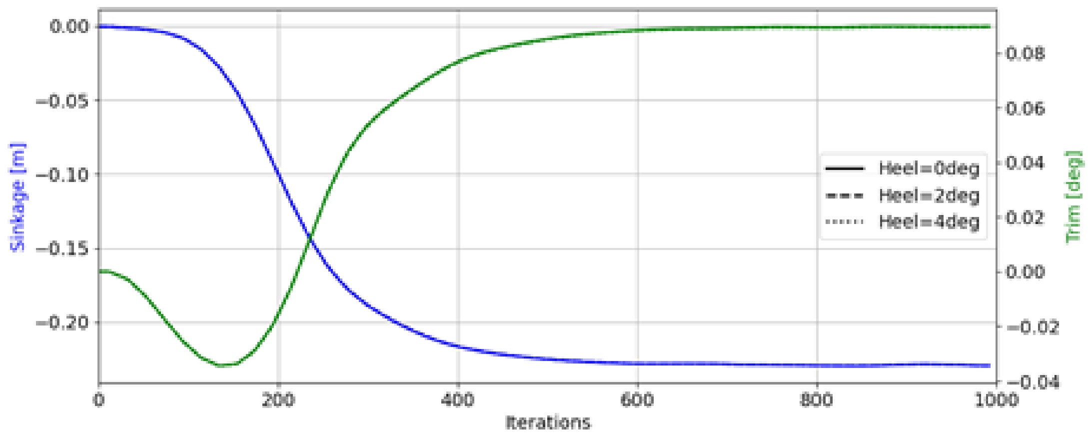


Attitudes of vessel

Figure 3: Resistance and attitude results for MV Kastor for various heel angles for $T_{sc}$=14.45m and V=14.0kn.

As shown, the differences in resistance are minimal and also, in all cases, the same convergence properties are observed. Additionally, the same pitch and heave trends are predicted. Since the vessel has a large block coefficient, the pressure field and the wave elevation around the hull are not affected by the heeling of the vessel and thus no differences in resistance are observed. Regarding the heeling moment that acts on the vessel, this has a pure hydrostatic nature and it is independent from the ship’s speed. The heeling moment can be acquired from the vessel’s trim and stability booklet (e.g. GZ-curves).

To gain a better insight into the effect of the heel angle in the flow around ship, the following flow visualizations are presented for heel angles 0, 3 and 5 degrees. Firstly, Figure 4 shows the pressure distribution on the bow of the ship, while Figure 5 presents pressure distribution on the surface of the rudder. No differences are noted among the plots, as similar patterns are observed at the free surface wave elevation given in Figure 6.

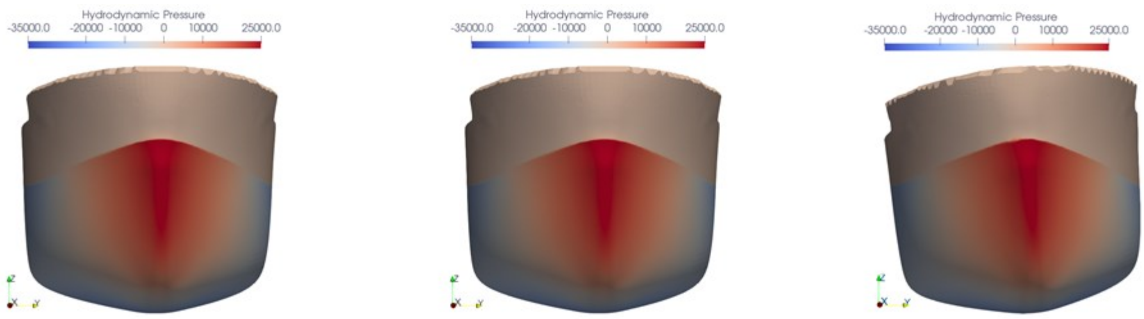


θ=0° θ=3° θ=5°

Figure 4: Contour of the hydrodynamic on the bow of the hull for $T_{sc}$=14.45m and V=14.0kn.

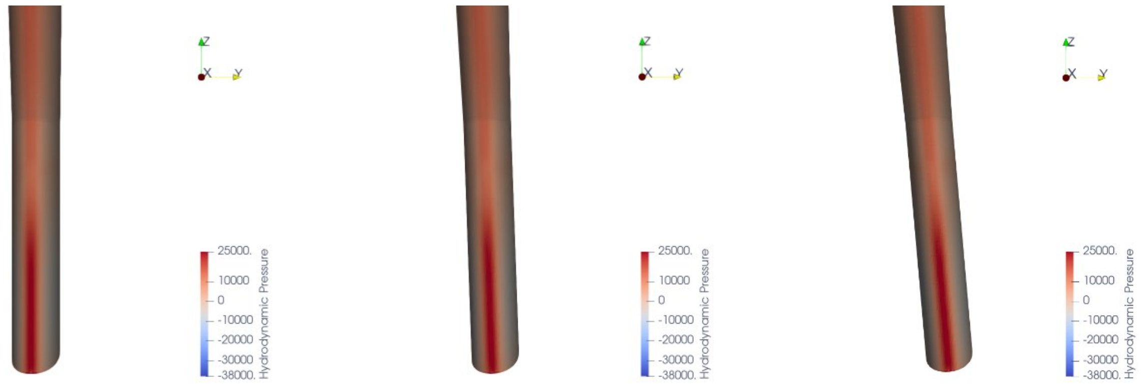


θ=0° θ=3° θ=5°

Figure 5: Pressure contour on the surface of the rudder for $T_{sc}$=14.45m and V=14.0kn.

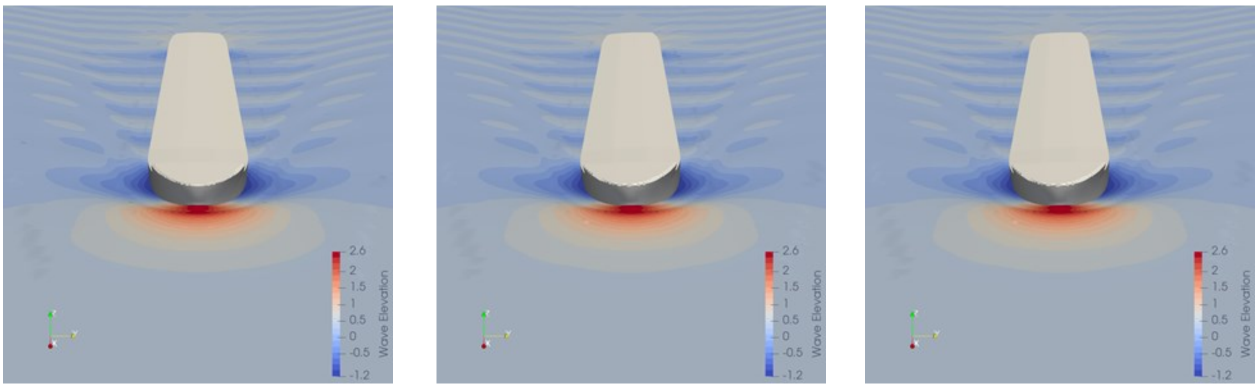


θ=0° θ=3° θ=5°

Figure 6: Free surface elevation for $T_{sc}$=14.45m and V=14.0kn.

Another key issue to consider when studying ships equipped with WASP is their impact on propeller performance. To examine the influence of the heel angles, the axial velocity component is presented in a plane close to the position of the propeller for 0, 3 and 5 degrees heel in Figure 7. Similar patterns are observed in all cases, thus no significant impact is expected at the performance of the propeller.

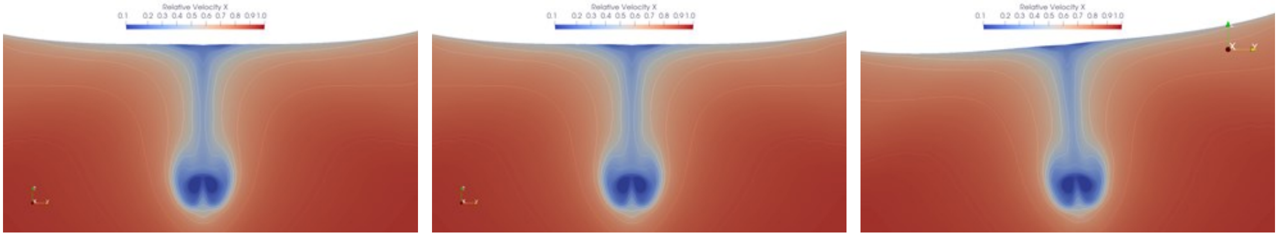

θ=0° θ=3° θ=5°

Figure 7: Relative velocity at propeller plane for $T_{sc}$=14.45m and V=14.0kn.

# 5 Hydrodynamic design considerations of ships in drift conditions

## 5.1 Systematic analysis of resistance, side force and yaw moment as function of drift

As shown in [1], in the case of standard merchant vessel hull shapes, the generation of side force and yaw moment in drift does not follow the behaviour predicted by wing theory applied to the hull. It is argued that this can be attributed to the extremely low aspect ratio of a ship (e.g. 14.4m draft by 220m length: AR = 0.065) compared to a typical lifting surface (AR >> 1). Furthermore, it appears that extrapolation of model test results to full-scale is not straightforward due to Reynolds number effects. While research on more accurate empirical predictions and transformation approaches is ongoing, in the meantime these properties must be determined by CFD simulations, ideally at full scale.

To provide input data for WP1 and performance predictions in WP4 a study on the generation of side force and yaw moment of the vessel *Kastor* at design draught (14.45 m), even keel and a speed of 11 kn has been conducted. The simulations were run at full scale on the bare hull using a bespoke version of OpenFOAM® [2] with a setup equivalent to the one described in D2.1.

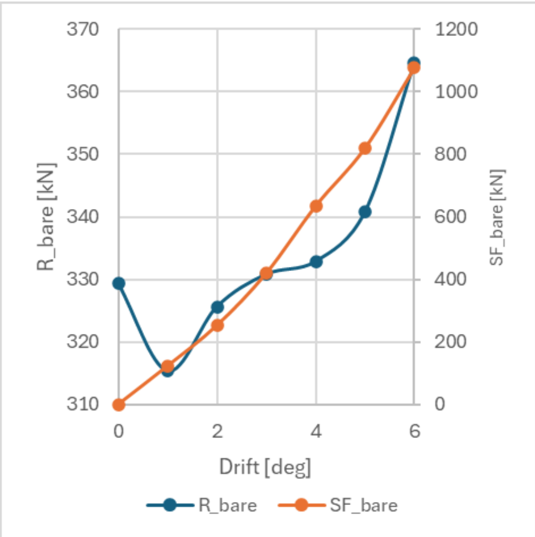


(a)

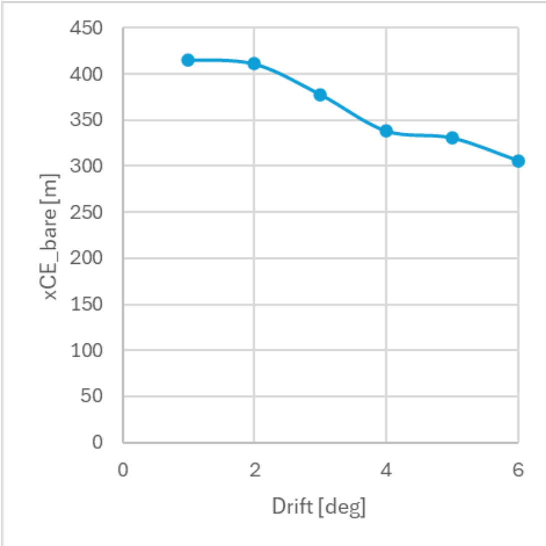


(b)

Figure 8: Forces and longitudinal center of effort (xCE), relative to aft perpendicular, as function of drift angle.

In **Errore. L'origine riferimento non è stata trovata.** the bare hull resistance (aligned with ship's longitudinal axis), side force (normal to ship's longitudinal axis) and longitudinal center of effort are depicted. The resistance (a) shows a behavior observed in other studies on similar hull shapes [1]. It appears that, at small drift angles, asymmetrically vanishing bilge vortices and beneficial interaction of waves from bow and forward shoulder may actually reduce the resistance. At larger drift angles the additional induced drag due the higher side forces generates a significant increase of resistance. For further analysis of this effect on systematically varied hull shapes please see [1]. The side force shows a linear behavior at small angle, up to 2°, as expected for a wing, with a super-linear behaviour at larger angles. This indicates that lift-creating vortices occur at the bilge radius (**Errore. L'origine riferimento non è stata trovata.**), similar to delta-shaped wings at high angles of attack.

The longitudinal center of effort (**Errore. L'origine riferimento non è stata trovata.** (b)) is located far forward of the ship, coming aft slightly with increasing yaw. This indicates the presence of a strong force-free yawing moment, the so-called Munk moment. This effect is currently being investigated in more details.

In **Errore. L'origine riferimento non è stata trovata.** it can clearly be seen that at higher drift angles, namely at  6,  two distinct vortices are shed:

- From the leeward (pressure) side a smaller vortex is shed, originating at the forward shoulder. This vortex diagonally transverses the bottom of the ship.
- From the bilge radius on the windward side a large vortex is shed, likely due to flow separation. This vortex rolls up the side of the vessel towards the stern.

Both vortices are visible in **Errore. L'origine riferimento non è stata trovata.**.

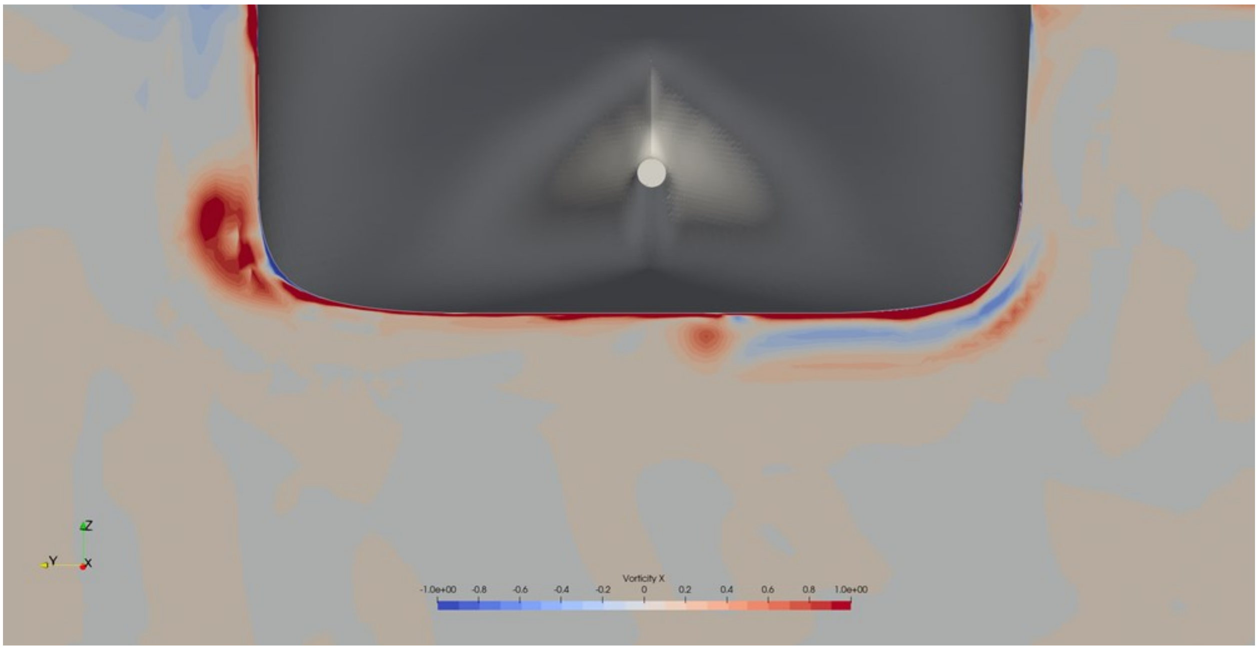


Figure 9: Vorticity-X on cutting plane 50m in front of aft perpendicular at 6° drift.

### 5.1.1 Surrogate modelling of drift-induced forces and moments

When focusing on similar ships (e.g. Kamsarmax-sized bulk carriers), surrogate models derived from one ship of that type can be used for analysis and optimization of forces and moments. For the vessel M/V KASTOR a further CFD-based study has been conducted varying draught, trim speed and drift angle in a quasi-random manner by Sobol distribution. This kind of sampling allows to consistently fill the parameter space with the least number of points. Further, as the distribution is described mathematically, it is fully reproducible. From this study the bare hull resistance and side-force as well as the longitudinal center of effort were calculated for the investigated conditions.

**Input Data**

- Bare hull geometry of MV Kastor
- Ship speed [kts], track-fixed
- Draught [m] at aft perpendicular

- Trim [m], negative bow-up
- Drift angle [deg]

**Output data**

- Resistance (bare hull) [kN], in ship coordinate-system (CL-aligned)
- Side-force (bare hull) [kN], in ship coordinate-system (normal to CL)
- Longitudinal center of effort (bare hull) [m]

**Methodology**

For further use Response Surface Models (RSMs) have been generated from the above results using the Kriging method from the Dakota software package [3]. These RSMs have then been re-sampled using a structured distribution of the input variables to generate look-up tables for inclusion in the DSS being developed in WP1.

**Operating condition space**

Table 5: Parameter space for Sobols and re-sampling.

| | nPoints | Draught_APP (m) | Trim (m) | Speed (kts) | Drift (deg) |
|---|---|---|---|---|---|
| 1st Sobol | 40 | 8 ÷14 | -3 ÷ 0.1 | 10 ÷ 15 | -0.5 ÷ 6.5 |
| 2nd Sobol | 30 | 6 ÷ 16 | -3.5 ÷ 0.6 | 8 ÷ 17 | -1.5 ÷ 7.5 |
| RSM | 1296 | 8 ÷ 14 | -3 ÷ 0.1 | 10 ÷ 15 | -0.5 ÷ 6.5 |

**Open issues**

During re-sampling the question of the necessary size of the Sobol parameter space versus the size of the re-sampling parameter space arose. Initial findings on similar sized parameter spaces put the viability of re-sampling results towards the boundaries in question. Re-sampling on an enlarged Sobol parameter space has shown a significant improvement in the plausibility of the results.

In Figure 10 the re-sampled response surfaces are visualized. For each operating condition shown two response surfaces are given per result parameter: in light blue for identical Sobol and re-sampling parameter spaces, in lavender for the enlarged Sobol parameter space. It can be clearly seen that the response surfaces in the middle of the parameter space are almost identical, whereas major deviations exist towards the parameter space boundaries.

Furthermore, in the side-force plots the SF = 0 line is shown projected on the base of the plot. Theoretically, this line should be consistently at a drift angle of 0°. Particularly in the uppermost plot a strong deviation can be observed. Enlargement of the Sobol parameter space has reduced but not removed this issue.

From the above it can be concluded, that the development of best-practices for the generation of surrogate models from a quasi-random distribution is still an ongoing topic.

The re-sampled response surfaces as shown have been provided to WP1 for inclusion in the DSS as base for the prediction of the hydrodynamic forces on the hull of the example vessel MV KASTOR when retro-fitted with WAPS.

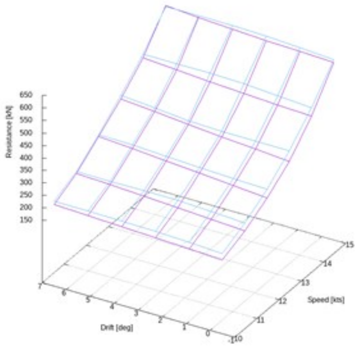

Resistance evaluated in minimum draught and maximum trim condition.

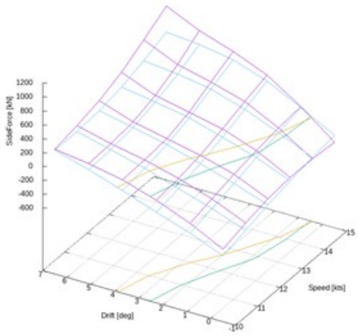

Side-force evaluated in minimum draught and maximum trim condition.

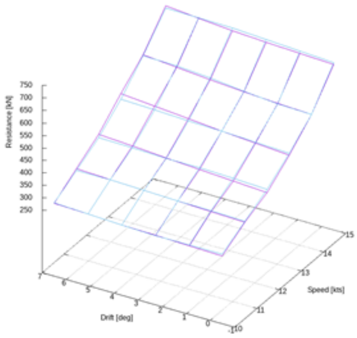

Resistance evaluated in medium draught and medium trim condition.

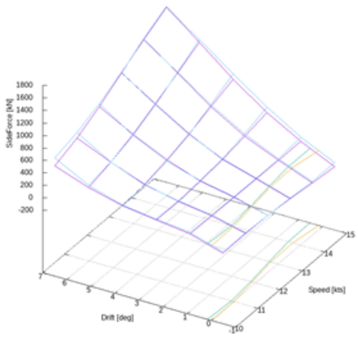

Side-force evaluated in medium draught and medium trim condition.

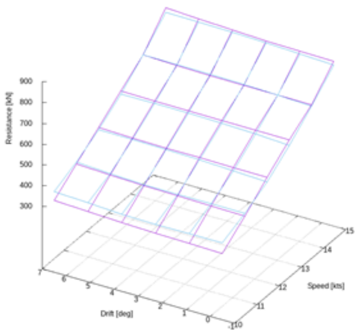

Resistance evaluated in maximum draught and minimum trim condition.

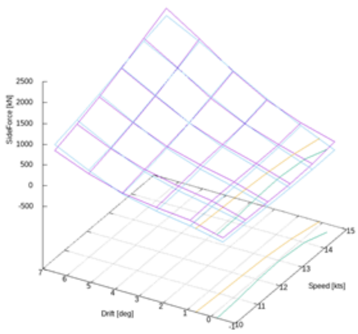

Side-force evaluated in maximum draught and minimum trim condition.

Figure 10: Visualization of resampled surrogate model.

## 5.2 Effect of ESDs in drift conditions

Although WASP is expected to significantly reduce the carbon footprint of ships, given the stringent targets set by the EU and IMO, the required GHG reduction can only be achieved through a combination of technologies. One of the most cost-effective solutions to improve the hydrodynamic performance of a vessel is the Energy Saving Devices (ESDs). This solution has been already examined consistently by various manufacturers and has already found its way into industry. Makers have reported gains up to 15%. ESDs aim to equalize the flow on the propeller plane by energizing the low-speed region above the propeller shaft.

This section aims to explore their hydrodynamic effect in drift conditions. To this purpose, SFD conducted five resistance simulations at different drift angles between 0 and 6 degrees. All simulations have been performed using Cadence/FineMarine v11.2. Details about the CFD setup can be found in deliverable D2.1. In order to examine the effect of the ESDs, a duct that consists of two half rings placed above the propeller shaft (Figure 11). This ESD has been selected for this study due to its promising results in self-propulsion simulations and is similar to designs already used by the maritime industry.

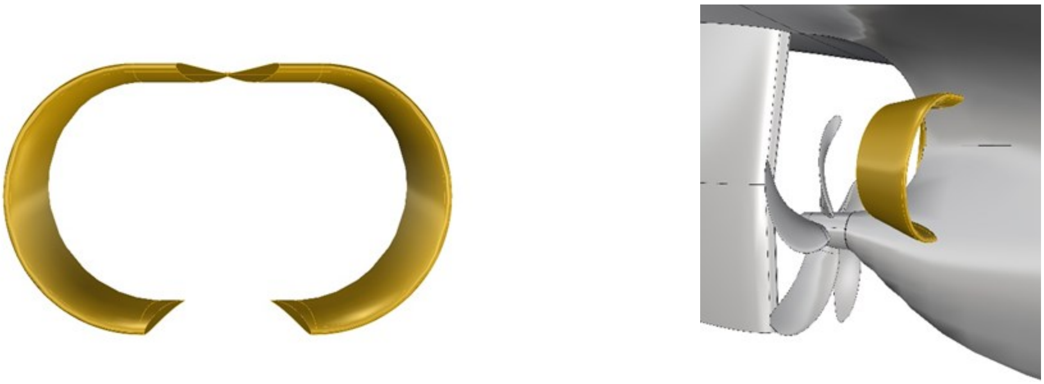

Figure 11: Duct with two half-rings fitted on the bulk carrier M/V Kastor.

Resistance simulations have been performed with and without the ESD. Firstly, in order to provide insight about the effect of drift angels on the hydrodynamic performance of the vessel, Figure 12 presents the wave elevation in straight ahead (β=0°) and in two drift conditions (β=3° and β=5°).

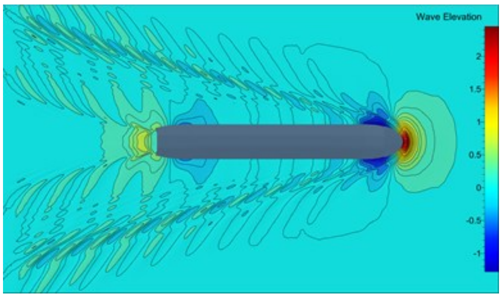


β=0°

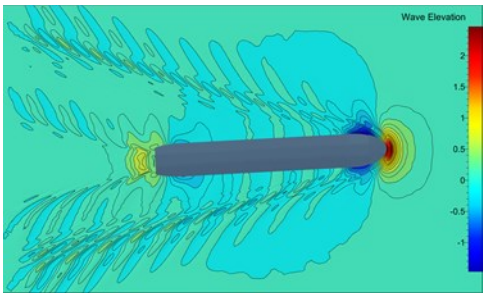


β=3°

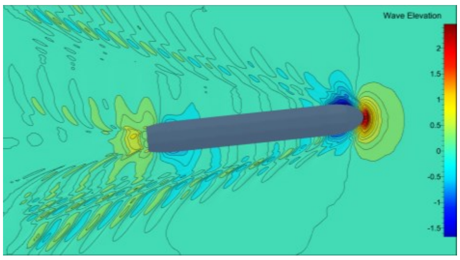


β=5°

Figure 12: Free surface elevation for different drift angles and for $T_{sc}$=14.45m and V=13.5kn.

Compared to the straight-ahead conditions, the wake is asymmetric and furthermore the wave amplitudes are large in the windward side and smaller in leeward side, as expected [4].

In Figure 13, the effect of the ESD on resistance and on side force is shown for five drift angles (β). Since the duct is symmetric, only positive angles are examined. In both cases, the resistance exhibits a quadratic trend with β, while the side force increases linearly. A larger resistance is found in presence of the duct, while a slightly smaller side force is noticed. By examining the distribution of the side force on the vessel (Figure 13, top-right), two spikes close to $x/L_{pp}$ equals 0 indicate the presence of the ESD. Similar to a wing with positive angle of attack, pressure increases in the bow of the ship due to the stagnation point. The acceleration of the flow at the after part of the ship causes a pressure drop and subsequently changes the sign of the transverse force. Overall, the distribution with and without the ESD is similar. Lastly, the drift moment is shown in the graph on the bottom, which scales linearly with the drift angle.

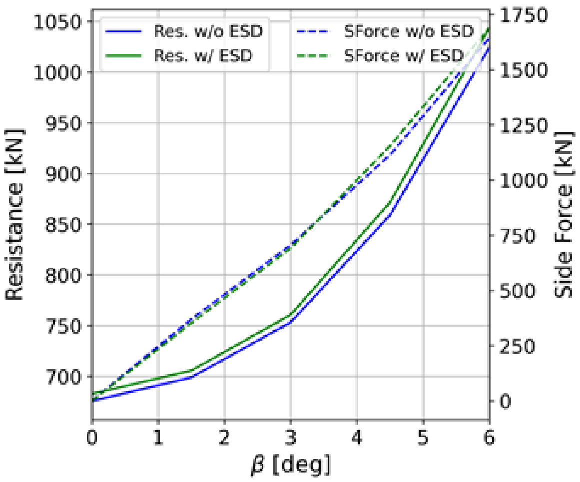


Resistance and side force.

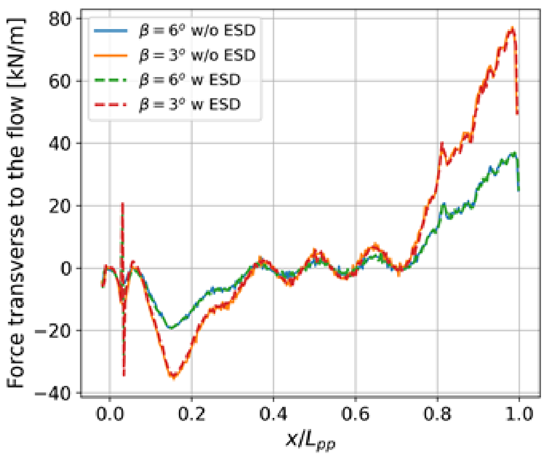


Distribution of the force transverse to the flow, for two drift angles, with and without ESD.

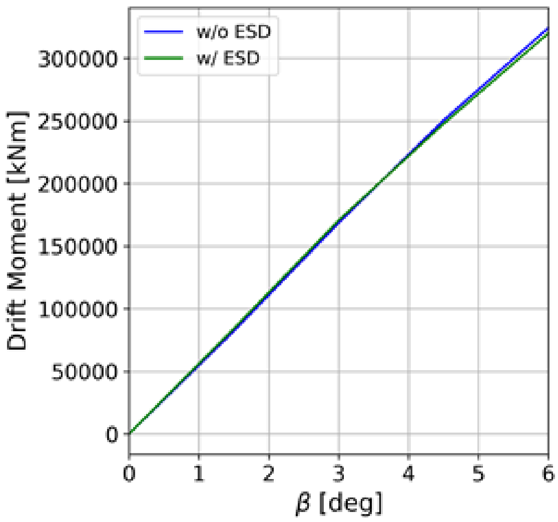


Drift moment.

Figure 13: Effect of ESD for different drift conditions and for Tsc=14.45m and V=13.5kn.

In addition to the hydrodynamic loads, we are interested in assessing the performance of the propeller in drift conditions with and without ESD. In Figure 14, the contours maps of the velocity deficit at the propeller disk are plotted for straight ahead conditions and for two drift conditions. The maps are provided for cases with and without ESD. Firstly, the wake at the propeller plane is asymmetric. The boundary layer becomes thinner in the windward side, while viscous phenomena become more intense at the leeward side with increasing drift angle. As shown in the following, an after body vortex is created at the stern tube of the vessel, which passes through the propeller disk. Furthermore, in the figures the wake deficit (w) is shown for each case. Although stronger viscous effects are observed for large drift angles, a small decrease in the wake fraction is noted. This is caused by the acceleration of the flow in the windward side. This will lead to an asymmetric loading of the propeller. Regarding the effect of the ESD, a stronger flow separation is predicted when the duct is present. It is likely that the cause is a misalignment of the duct with the flow.

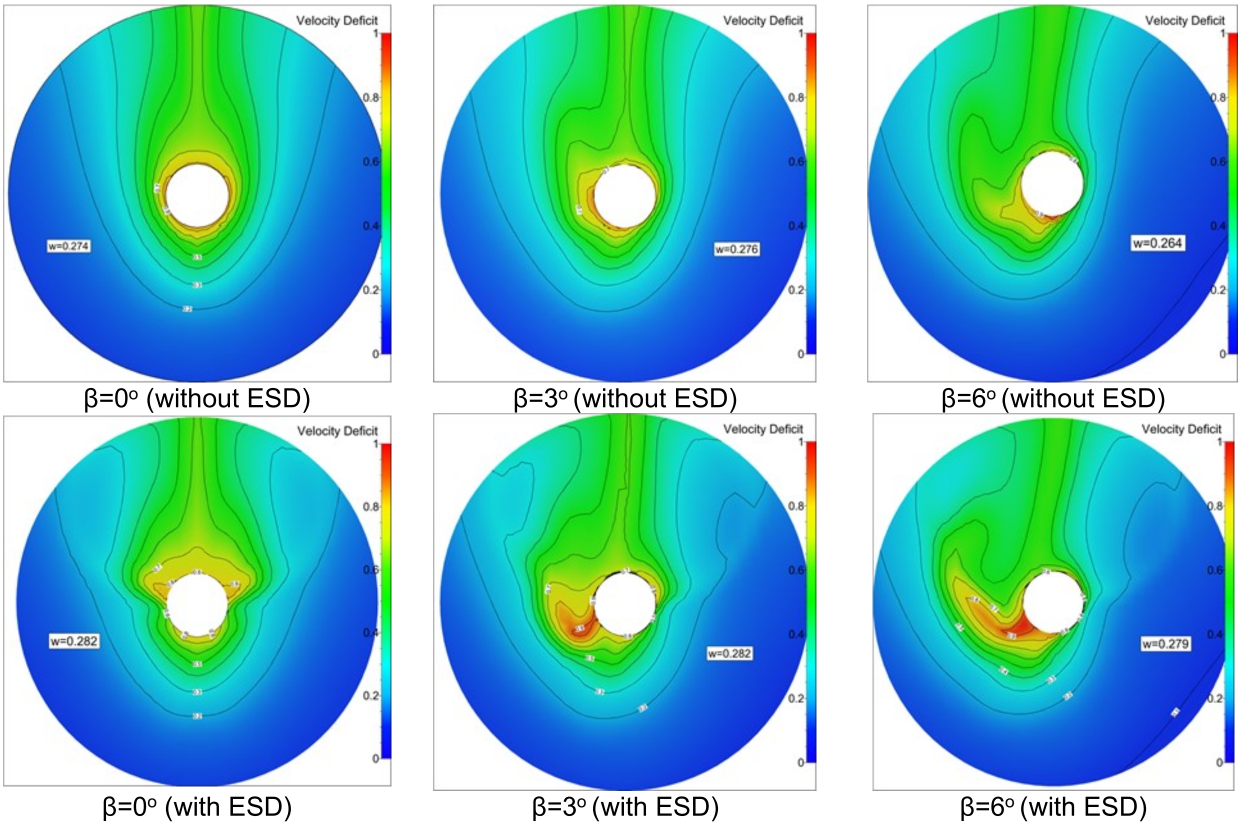


Figure 14: Contour of the velocity deficit at the propeller plane disk influenced by the presence of a duct with two half-rings in drift conditions.

In order to gain a more in-depth understanding of the flow conditions in drifting situations, an examination of the vortical system created under the hull is conducted. When a ship is sailing in drift conditions, a specific system of vortices is created beneath the hull [4]. This vortical system is illustrated at β=6° on the bare hull and in the case of the hull equipped with ESD in Figure 15. A strong aft bilge vortex (ABV) is apparent, which affects the stern wake and the distribution of the axial velocity component.

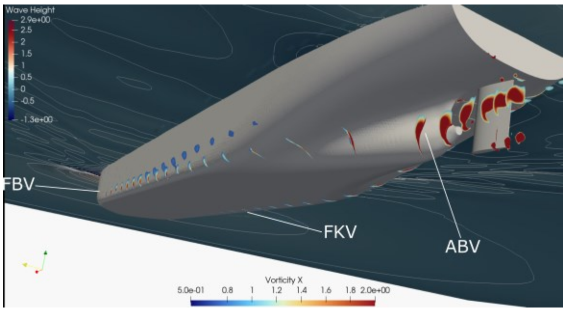

Without ESD.

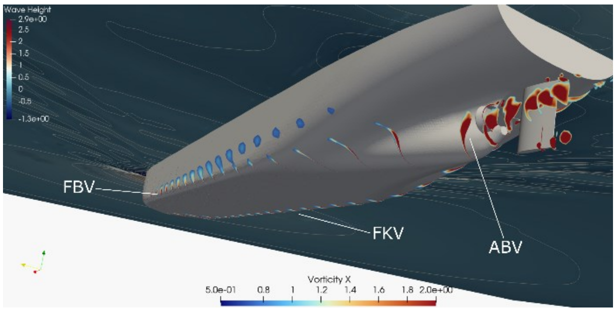

With ESD.

Figure 15: Flow visualization of vortex system created in case of β=6°.

## 5.3 Analysis of influence of speed, draught, trim and drift on the nominal wake field in presence of an existing pre-swirl duct

The impact of an ESD on the study vessel may be changed or even be cancelled in the presence of a trim or drift angle. As designed, the fins of the pre-swirl duct act as lifting surfaces. This modification of the alignment of the incoming flow into the propeller, in addition to the induction of pre-swirl, serves to reduce the required propeller revolutions. Due to trim or drift angle of the ship, the inflow angle into the ESD may change to the point where the angle of attack of the fins is greatly altered or even reversed.

In order to evaluate these effects, a parameter space consisting of speed, draught, trim and drift has been analysed using a Design of Experiment approach, and the corresponding viscous CFD simulations have been run.

### 5.3.1 Existing pre-swirl duct

The vessel *Kastor* is fitted with a pre-swirl device consisting of a circular converging duct centered on the propeller shaft and equipped with five fins with asymmetric wing sections (Figure 16).

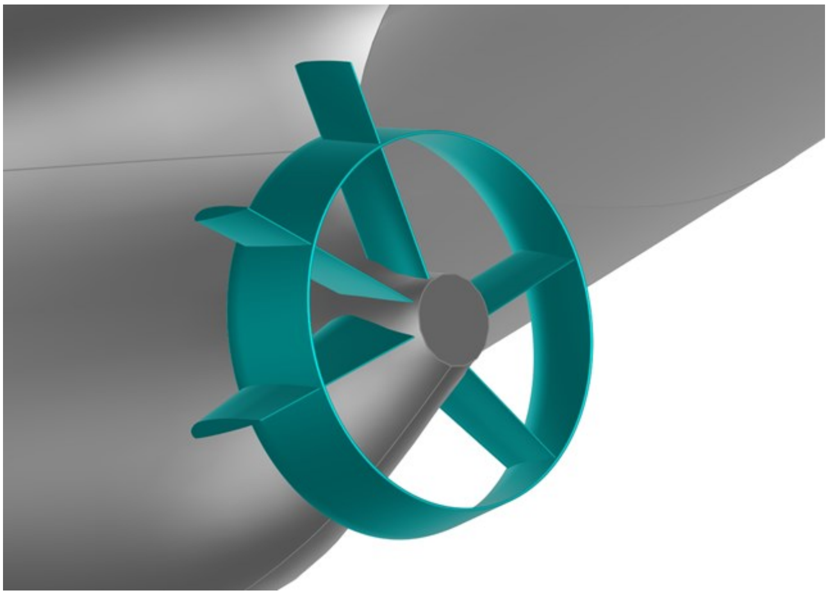

Figure 16: Pre-swirl duct fitted to Kastor.

The purpose of such ducts is to homogenize the inflow by reducing the effects of the boundary layer and stagnation zones on the hull. The fins are used to generate the pre-swirl – a rotation of the wake field. To this purpose, the fins are designed to operate at a particular angle. Under design conditions, according to the towing tank test report [5], the energy savings due to the pre-swirl duct are of about 6%, which results in a reduction of the propeller revolutions of about 3.8%.

### 5.3.2 CFD-Simulations and DoE

To evaluate the nominal wake filed in presence of the pre-swirl duct, viscous CFD simulations in model scale and using the same setup as those described in Section 5.1 have been carried out at different draught, trim, speed and drift, following a Design of Experiment (DoE) approach, to evaluate the effect of the different parameter combinations. A total of 20 test cases were simulated, with the parameter space boundaries as shown in Table 6.

Table 6: Parameter range for evaluation of ESD.

| | Draught | Trim | Speed | Drift |
|---|---|---|---|---|
| Min | 6.30m | -3.0m | 10.0kn | -6.0° |
| Max | 14.45m | 0.0m | 15.0kn | 6.0° |

### 5.3.3 Evaluation of the nominal wake field

To evaluate the wake field, several descriptive values and their standard deviations have been computed for the flow through the propeller disk, such as the Taylor wake fraction, which is defined as

$$w = 1 - \frac{u_{Avg}}{u_{\infty}}$$

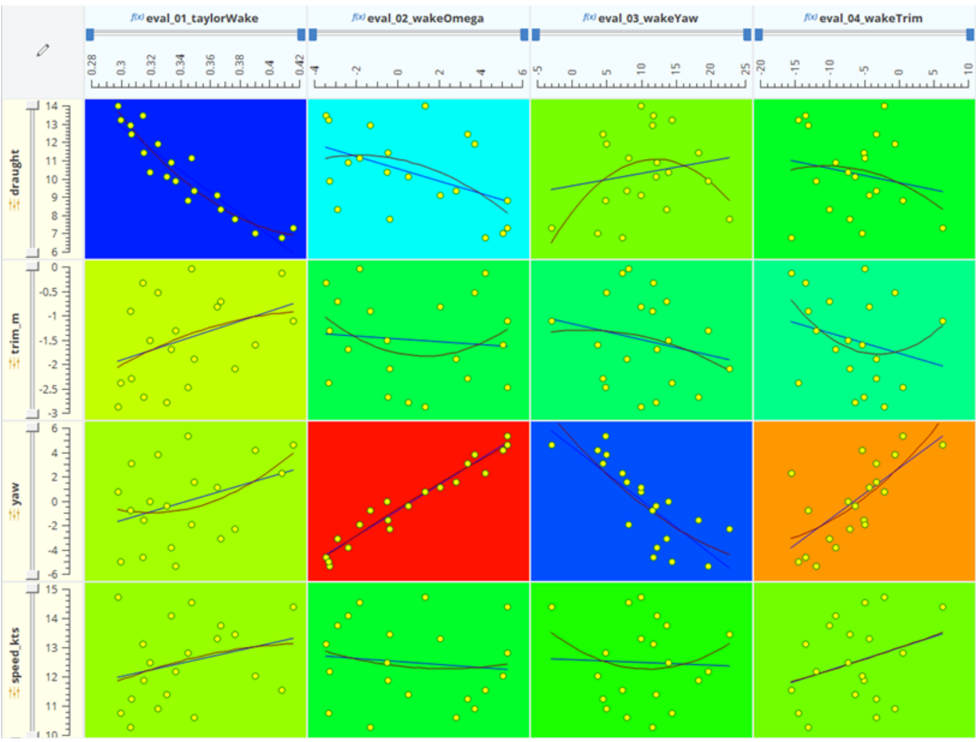


Figure 17: Correlations between operating conditions and wake field.

The average yaw and trim angles of the wake, as well as the average rotation rate have been computed.

In Figure 17 the correlations between the operating conditions and the computed average values describing the wake field are shown. It is particularly evident that – besides the dependency of wake fraction on draught – the drift angle has a significant impact on direction as well as on the rotation of the wake field. This is particularly relevant for a WASP-equipped vessel that will operate at drift most of the time due to the side force generated by the WASP system.

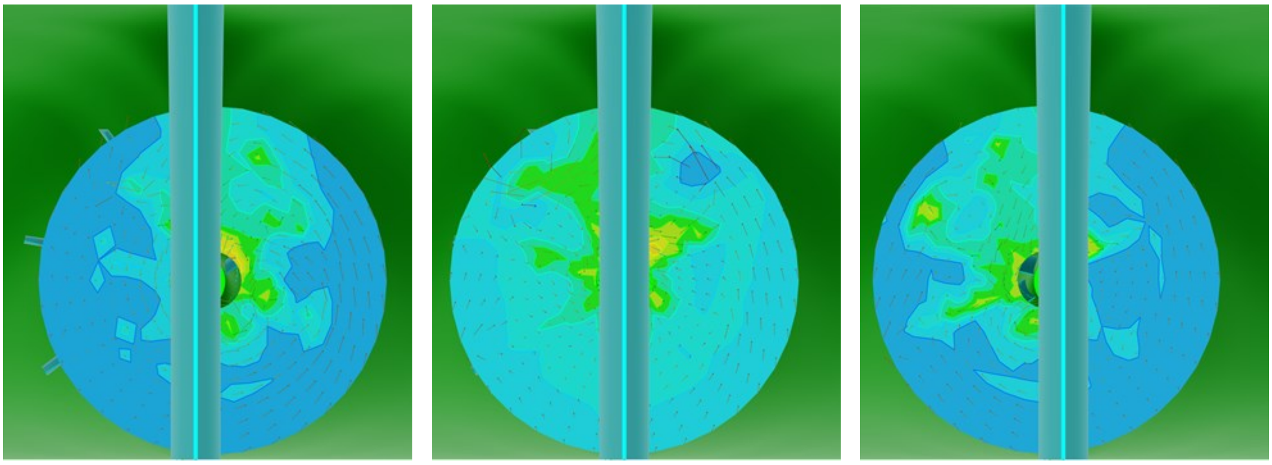

Yaw angle = -5.3° Yaw angle = 0° Yaw angle = 5.3°

Figure 18: Wake field at different yaw angles.

Figure 18 illustrates the wake field for different yaw angles. The figure clearly demonstrates the variation in the relative length and orientation of the in-plane flow vectors, as well as the change in velocity distribution. These observations provide further support for the conclusions previously outlined.

# 6 Hydrodynamic design optimization of ship with WASP

As a preliminary study to the optimization of actual vessels, a study on retrofitting of parts of the hull for operation with WASP has been conducted on a canonical hull shape. The well-documented KVLCC2 test case ([5] and [6]) has been chosen. The simulation setup has been the same as that described in Section 5.1. The evaluation methodology is documented in [7], [8] and [9] and the detailed results are documented in [1].

## 6.1 Scope of optimisation

To evaluate and optimize the hull geometry of the chosen vessel, the existing CAD model of the hull has been imported into the platform CAESES [10] and parametric modifications applied to the forebody and aftbody region.

### 6.1.1 Forebody

In absence of a fully parametric hull model, having a direct dependency of the hull shape on a set of design parameters, a semi-parametric morphing region has been applied to the region of the stem that might typically be replaced by a bulbous bow retrofit as shown in Figure 19. Semi-parametric morphing means that the space inside the box shown in Figure 19 is deformed proportionally with deformations of this box, resulting in a deformation of the hull shape within this box. This approach allows modification of the shape in this region while maintaining curvature continuity at the boundary of the morphing region. The range of possible modifications is shown in Figure 20.

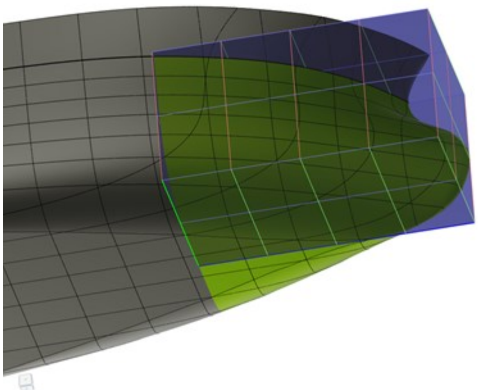

Figure 19: Morphing region for stem modification.

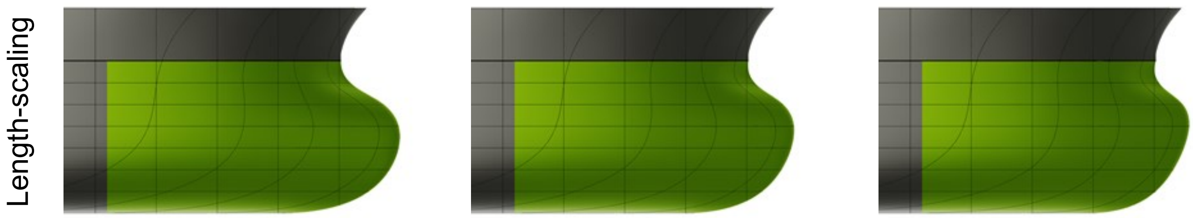

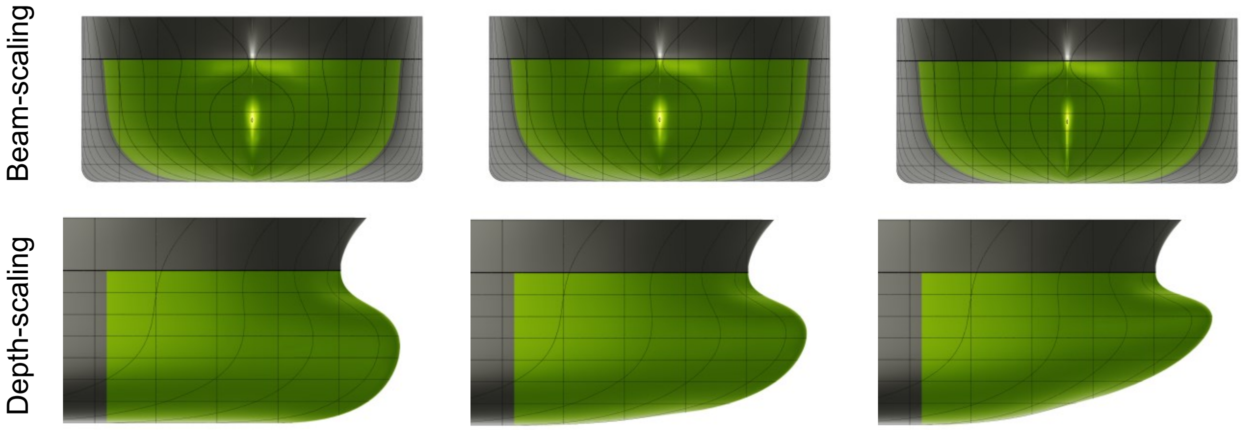


Figure 20: Investigated parameter range for stem modification.

### 6.1.2 Deadwood

The deadwood is added as a parametrized object and merged to the existing hull. The range of variations is shown in Figure 21.

Figure 21: Deadwood extensions investigated.

### 6.1.3 Design of experiment

The effect of stem morphing on the flow properties and resulting forces / moments has been evaluated by a Sobol-based Design of Experiment approach, to efficiently cover the possible design space and allow the generation of response surface models for optimisation. In total 20 stem designs have been investigated at drift angles of 0°, 3° and 6°.

## 6.2 Results

From Figure 22 to Figure 24 the coefficients of residual resistance, added resistance due to drift and side force are shown as a function of drift angle, for selected hull designs.

Figure 22 presents residual resistance, i.e., the total resistance with the frictional part deducted relative to the corresponding values of the baseline hull. It is shown that the baseline hull has one of the highest resistances of all variants, when evaluated with 0° drift. At this condition, one of the variants generated by the DoE-approach (called des0014 in Figure 22) features a residual resistance which is a whole 15% less than the value of the baseline hull. However, at 3° and 6°drift, the baseline hull is one of the best. This indicates that the forebody has a huge impact on not only the resistance at 0° drift, but also on the additional drag that results from drifting. The total resistance at full scale varies by up to 9.8% at 0° and 6% at 6° drift.

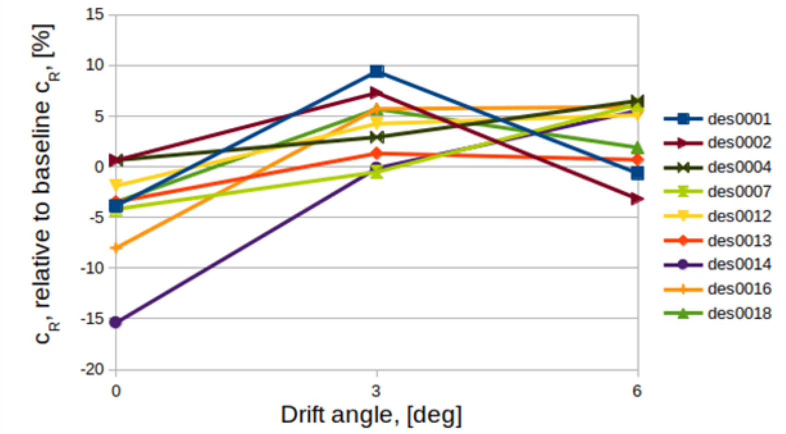


Figure 22: Residual resistance at 0, 3 and 6 deg of drift, relative to the baseline values.

A closer look at the added resistance due to drift is provided in Figure 23, where the values evaluated by the ChaSE platform are shown for comparison. The ChaSE platform evaluates the side force and drag based on an approach combining low aspect ratio wing theory and cross flow drag [7]. It is shown that the behaviours of the actual hulls' resistances differ largely. Some hulls, e.g., the baseline hull, have a negative added resistance at 3 degrees of drift with negligible added resistance at 6 degrees. Other hull variants have large added resistances at 3 degrees of drift, but little added resistance at 6 degrees of drift (e.g. des0001). Two hull variants show almost linear behaviour with increasing added resistance over the drift angle, namely des0014 and des0016 (as named by the CAESES design engine). It is also shown that the values evaluated by ChaSE are rather high, but within the group of hulls up to 3°. However, at 6° of drift the added resistance is overpredicted by ChaSE for all hull variants.

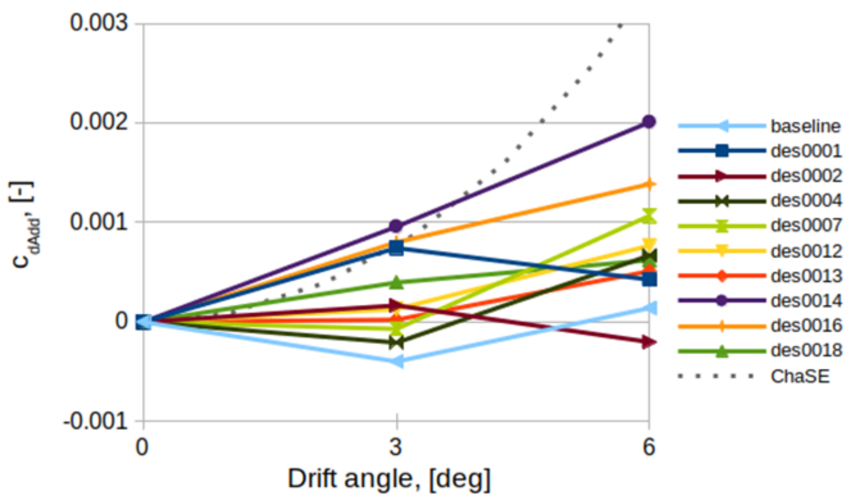


Figure 23: Added resistance due to drift.

Unlike the resistance, the generated side force differs only slightly between the variants, as shown in Figure 24. A maximal difference of less than 4% is observed at 6° of drift. The value estimated by ChaSE is slightly conservative as it is below the entire cluster of design variants by more than the spread of this cluster.

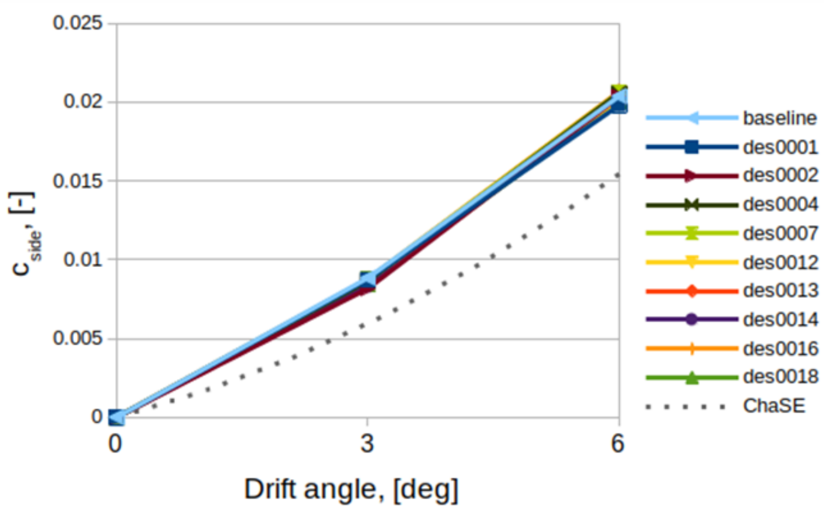


Figure 24: Side force generated by the drifting hulls.

To investigate the different additional resistance of the hull variants, two variants are selected to be compared to the baseline in more detail. The selected variants for this comparison are des0007, i.e., a design with no added resistance at 3° but rather high added resistance at 6° drift, and des0014, i.e., the one design featuring an almost linearly increase of added resistance with drift.

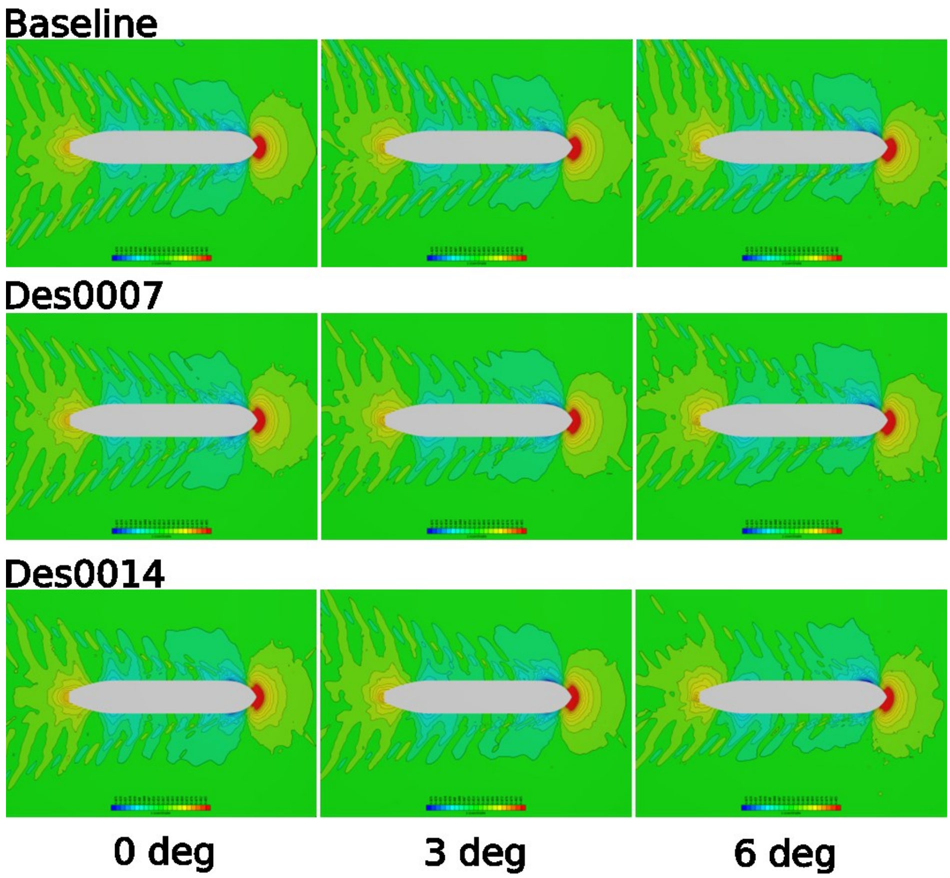


Figure 25: Wave patterns of the baseline, des0007 and des0014 at 0, 3 and 6 degrees of drift.

As a first step, Figure 25 compares the wave patterns of the three variants at the different drift angles. Variant des0007 appears to have a favourable interference on the “suction” side, which can cause the phenomenon that the resistance does not increase between 0 and 3° drift. This interference seems to vanish at 6 degrees, thus explaining the increase of resistance between 3° and 6°. The wave pattern of variant des0014 does not change much between 0 and 3 degrees, but the free waves are considerably lower on the suction side at 6°. However, a large wave trough is created at the bow T 6° drift Thus, the influence of the free surface on the added resistance seems to be smaller for this design. It can also be seen that des0014 has much reduced wave pattern compared to the baseline and the des0007 variant at 0° drift, explaining the lower resistance. The baseline features almost constant wave patterns for all drift angles, thus the drop in resistance at 3° drift cannot be explained from the free surface plots.

As a second step, the pressure distribution (dynamic pressure) at the forebody is compared in Figure 26. The baseline shows a much less pronounced field of negative dynamic pressure at the transition to the flat of bottom compared to the other variants. At 3 °drift, the low pressure at the forward shoulder on the pressure side is reduced, which might help with decreasing the resistance. At 6°drift, a pronounced low pressure at the bottom is formed, which could result in some separation in this area, thus causing additional resistance. The trends are identical for the other hulls. However, the more pronounced fields of negative dynamic pressure on the bottom could give earlier separation, thus increasing the resistance, especially for des0014, which also features a large area of negative dynamic pressure at the forward shoulder of the suction side, as discussed earlier.

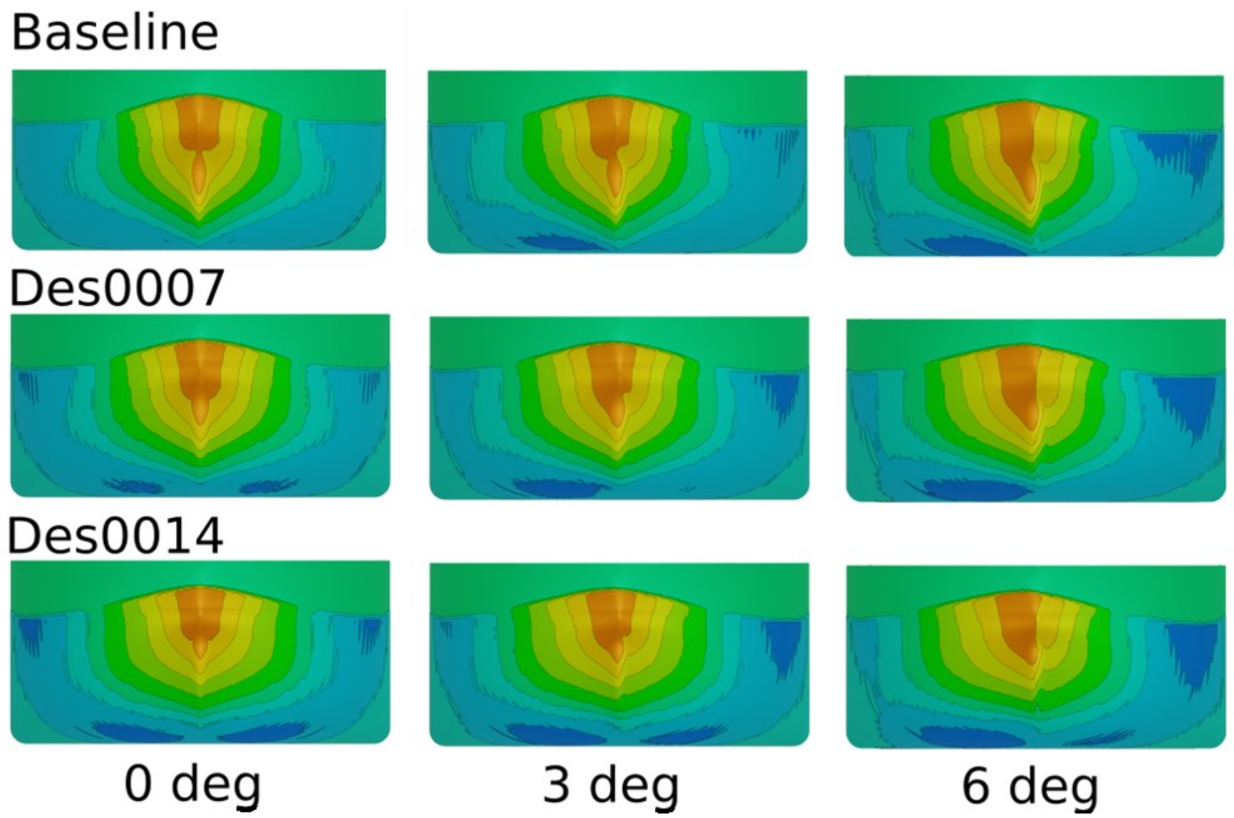


Figure 26: Pressure distribution (dynamic) at the bow of the baseline, des0007 and des0014 at 0, 3 and 6 degrees of drift.

In summary, the side force of a drifting hull seems to be mainly created by vortices formed around the bilge and the centerline of the hull. The forebody variations have only minor effects on the side force. **The additional drag is influenced by a variety of factors, making it challenging to predict**. At a drift angle, the bilge vortex can vanish in the skeg region, which will decrease the resistance. A favourable (or unfavourable) interference might occur in the free surface wave pattern of a drifting ship and the low pressure fields at the transition from the bow to the flat of bottom become more pronounced when drifting. ChaSE has estimated the values to be accurate in magnitude, but the figures are more conservative than those of the ship. For drift angles larger than 3°, the drag is overpredicted.

The effect of the deadwood in the stern region on the side force and added drag was estimated by creating two variants with different deadwood sizes. The side force and added drag relative to the side force and added drag of the baseline are presented in Figure 27. The results show that the deadwood considerably increases the created side force but also increases the additional drag. The increase in drag and side force are most pronounced at 3°drift. One hypothesis for this phenomenon is that the presence of deadwood generates a robust vortex at lower drift angles, which is subsequently amplified at larger angles, even in the absence of deadwood.

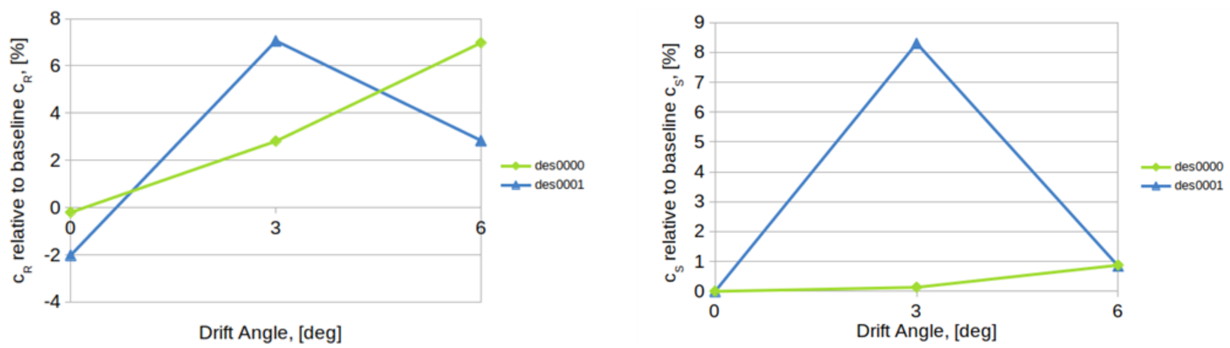


(a) (b)

Figure 27: Residual resistance (a) and side force (b) of the variants with a deadwood relative to the baseline values.

To illustrate the effect of the deadwood, the turbulent kinetic energy (TKE) in the stern region is presented in Figure 28.

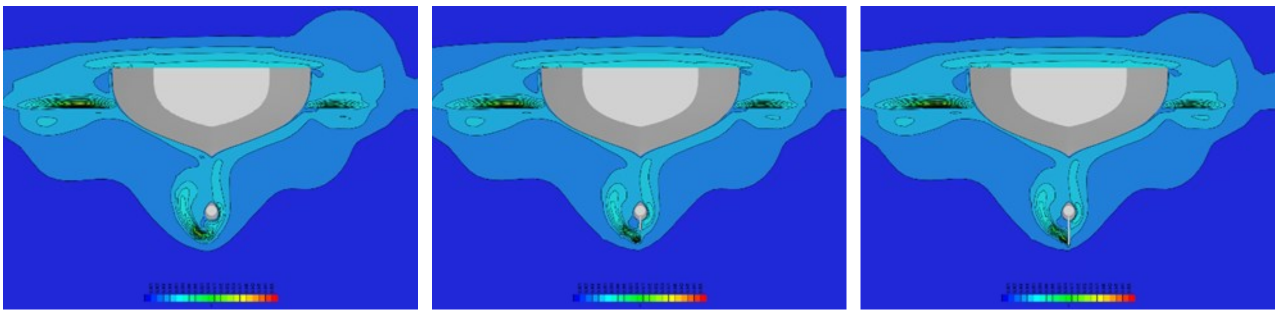

Figure 28: TKE at deadwood at 3° drift (left to right: baseline, increasing extension).

The effects of both the stem morphing as well as the addition of a deadwood are evaluated in ChaSE for a canonical WASP setup. Three variants are selected for comparison of the stem modification: the baseline hull, which features a very low drag at 3 degrees of drift, des0014 which has the lowest drag at 0 degrees of drift and des0016, which has the highest side force at 6 degrees of drift. Both hull variants have considerably lower resistance at 0° drift, compared to the baseline but higher resistance at 6°. The required propulsion power from the propeller is compared in true wind angles (TWA) between 0-180 degrees and true wind speeds (TWS) of 5 and 20 kn. The results in terms of relative power (PD over PD-baseline) are presented in Figure 29.

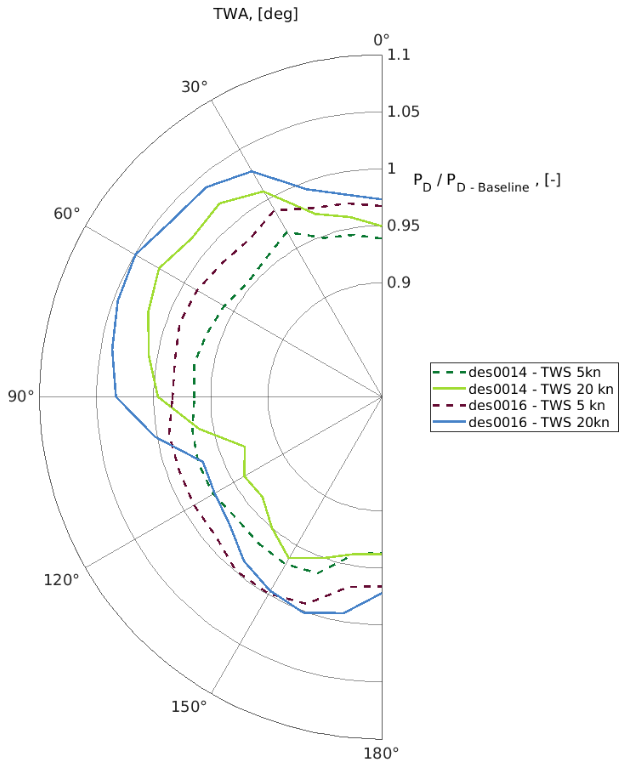


Figure 29: Polar plots of the required propulsion power from the propeller relative to the required power of the baseline hull.

The results show that both hull variants require less power at low wind conditions, which is down to their lower resistance without a drift angle. However, when wind speeds reach 20 knots, the hull variants are preferable in all wind angles, provided that the sails do not generate significant side forces, thereby preventing the vessel from drifting.  However, in higher wind speeds, the higher added resistance due to drift seems to dominate in cases where large sideforces are generated by the sails (and have to be countered by the hull and rudder). This is observed at TWA between 0-30 degrees and 110-180 degrees. In the TWA range of 30-90 degrees, both hull variants are up to 5 percent worse. Obviously, the slightly larger side force (observed for the hull variant des0014) does not affect the total performance as much as the higher drag.

As for the forebody variations, the effect of the deadwood on the performance of a WASP ship is evaluated using ChaSE at the same conditions. The results presented in Figure 30 show that the variants with a deadwood are worse in most conditions. As for the bow variations, this shows that it is more important to reduce the drag at drift than to increase the lift.

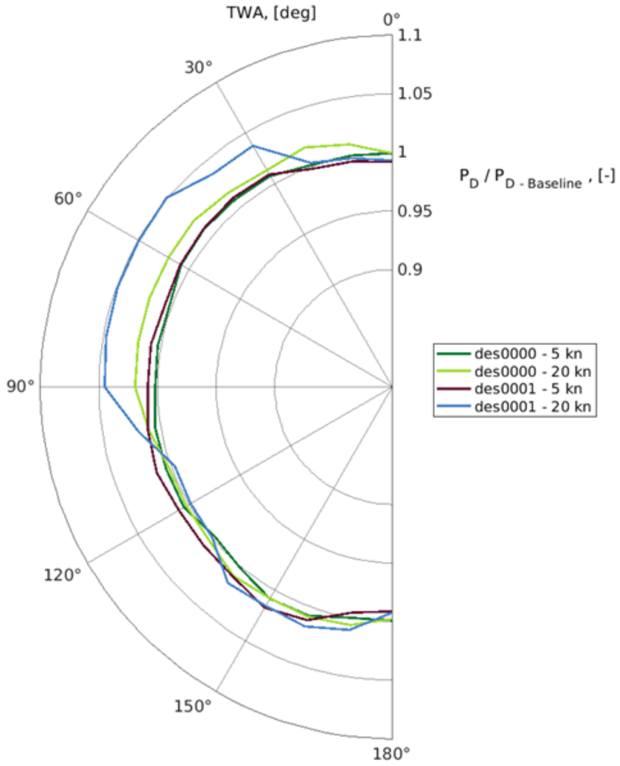


Figure 30: Polar plots of the required propulsion power from the propeller relative to the required power of the baseline hull.

# 7 Open water rudder tests

The installation of a WASP system has a significant impact on the vessel's dynamics. Aerodynamic forces due to wind and hydrodynamic forces due to the motion of the vessel should be balanced to allow for the efficient course keeping of the vessel. If aerodynamic and hydrodynamic forces act on the same point, i.e. the aerodynamic center of pressure and center of lateral resistance are on the same position. Equilibrium of aerodynamic and hydrodynamic forces is a necessary condition for maintaining a constant ship speed. In case the aerodynamic center of pressure and the center of lateral resistance do not act on the same point and a horizontal distance exists between them, the vessel will turn to weather or lee unless a rudder force is introduced [11]. As a result, the action of the rudder will introduce additional resistance. In order to compute the rudder angle that is required in each case to maintain the ship course, the full set of the aerodynamic and hydrodynamic components is needed.  The purpose of this chapter is to provide the necessary hydrodynamic characteristics of the rudder of the specific bulk carrier vessel and to export them to WP7, where the assessment of weather routing tool for the specific bulk carrier vessel equipped with WASP takes place.

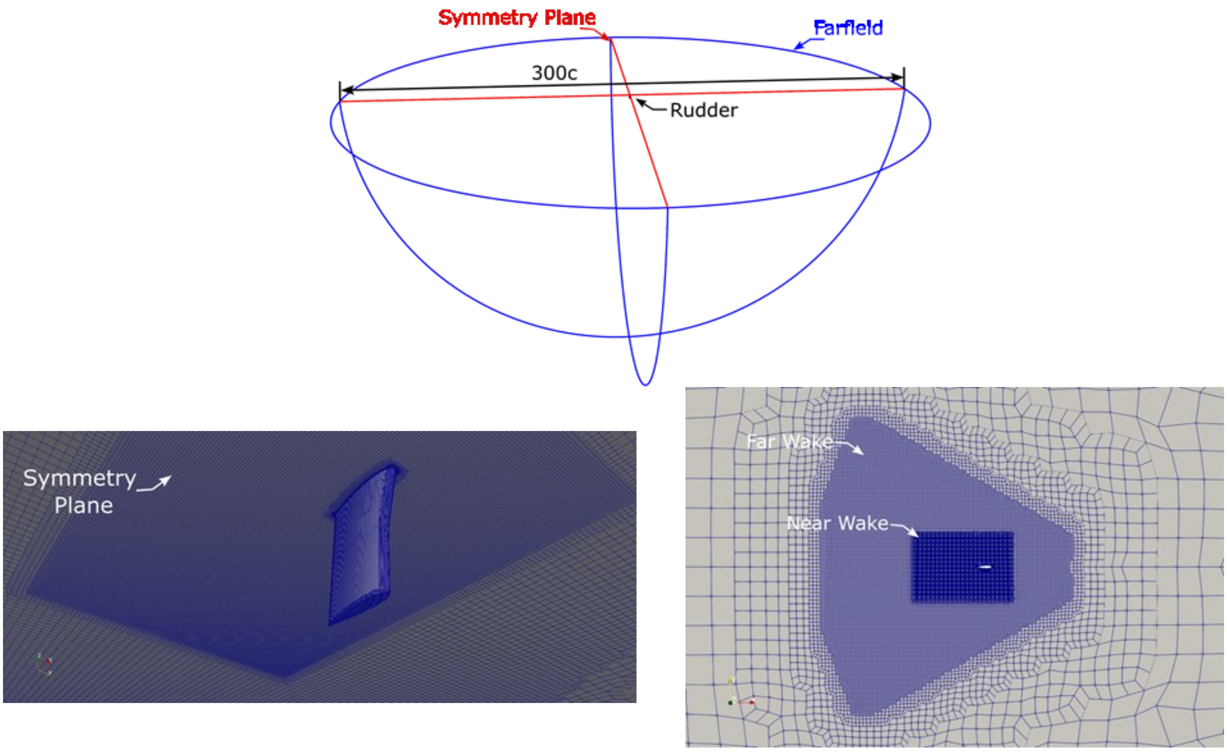


Figure 31: Computational setup for open water rudder tests.

The hydrodynamic performance of the M/V Kastor’s rudder is examined using open water tests. The rudder is isolated from the hull and is examined for a range of angle of attack (AoA), between 0° and 25°. The Reynolds number is 35 million. This corresponds to inflow speed equals to 13.5kn for the full scale condition. The computational domain is depicted in Figure 31 (top). Since the effect of the free surface is neglected, symmetry boundary conditions are considered on the top boundary. A half circle domain of large radius is selected to ensure that no reflections occur at the far-field boundary. Two mesh regions with increased refinements are employed to ensure an adequate resolution of the pressure field around the rudder, as shown in Figure 31. Wall functions are used to resolve the boundary layer. The first node is placed 0.0008 m away from the wall in the normal direction, which results in $y^+$ below 30 in all cases.

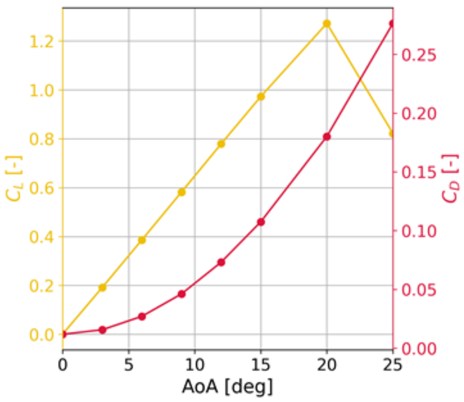


Figure 32: Results of open water rudder tests. Lift (CL) and drag (CD) coefficient for Re=25 million.

In Figure 32 the results of lift and drag coefficients are shown. $C_L$ scales linearly until 20°, where a stall region appears. $C_D$ has a quadritc behavior, as expected. Flow visualization plots are shown in Figure 33 and Figure 34 for the cases of 0°, 9°, 20° and 25°. The flow is attached to the whole surface of the rudder for the first two cases. In the third case separation occurs at the lower region of the rudder, whereas in the last case a large separation region is evident.

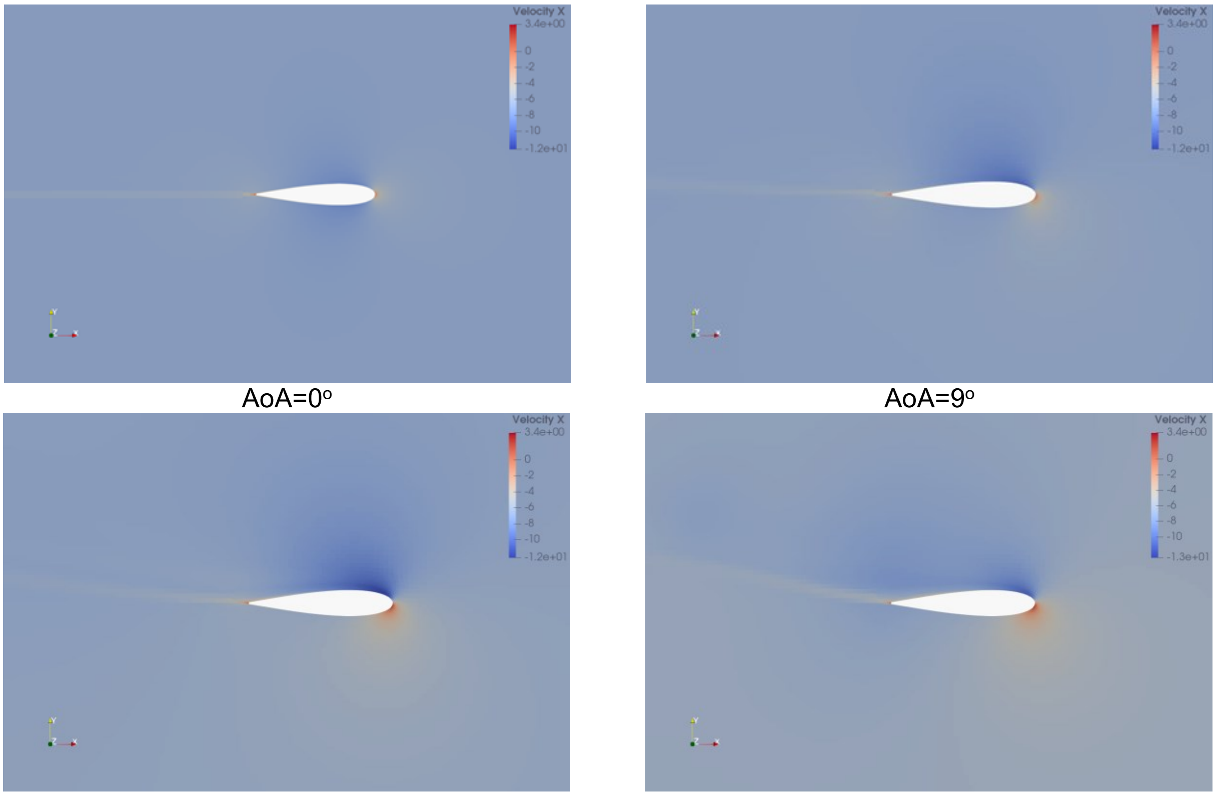

AoA=0° AoA=9°

AoA=20° AoA=25°

Figure 33: Axial velocity contours on symmetry plane.

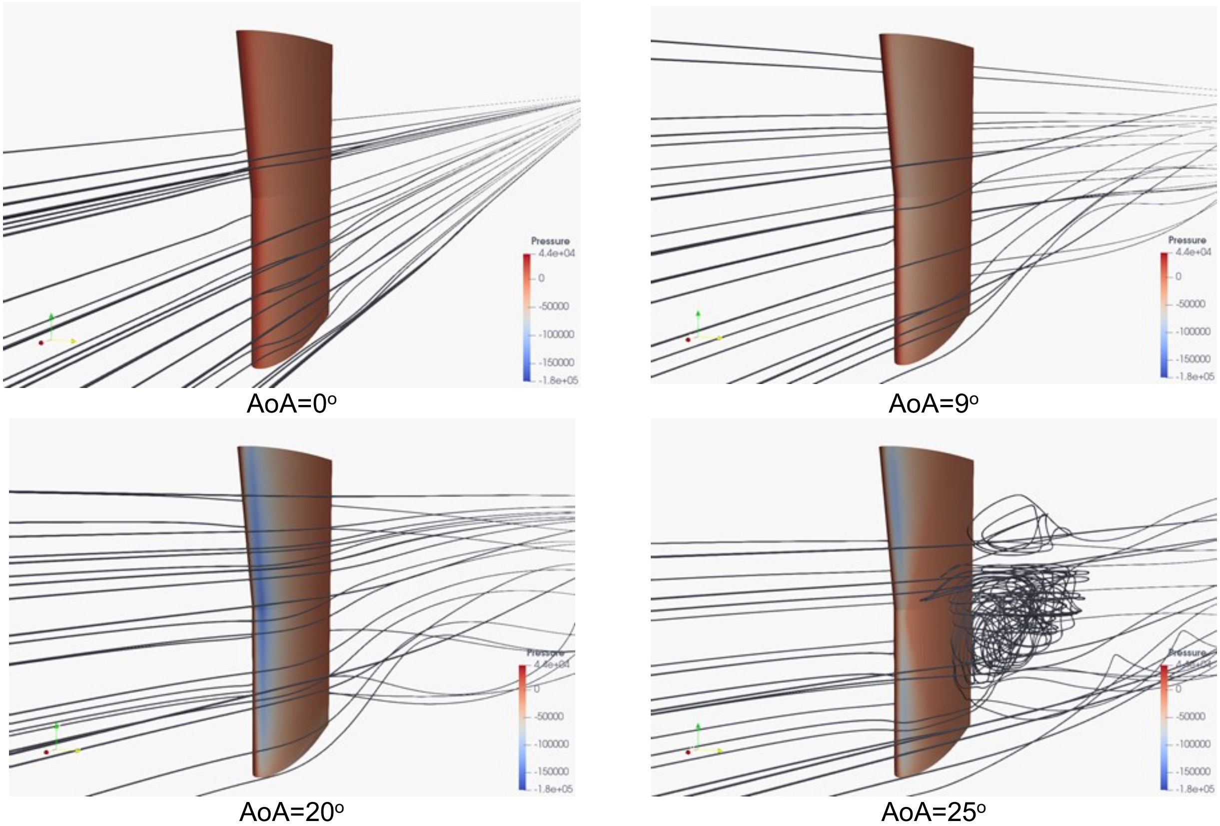


Figure 34: Flow visualization of open water rudder tests. Streamtraces and pressure contours on the surface of the rudder.

# 8 Closing remarks

The present report focuse*s* on the hydrodynamic aspects of the ship hulls when equipped with a wind assisted ship propulsion system.  A wind propulsor induces heel and drift angles to the ship. Taken as reference a Kamsarmax-size bulk carrier vessel, systematic studies have been carried out to explore their effect on the resistance and propulsion efficiency.

Firstly, it has been shown that for this type of vessel the effect of the heel angle is minor and can be neglected. The expected range of heel angles is below 5°, which is small and does not affect the pressure distribution, the wetted surface or the wave field behind the hull*.* This is *probably attributed* to the high block coefficient of the vessel. *However, it needs to be mentioned that, i*n other types of vessel*s*, further investigation is *necessary*. Regarding the effect of drift angle, in the present report*,* two studies have been included that both support a significant increase of the resistance of the vessel. A quadratic increase in resistance with respect to the drift angle is predicted. When the hull operates *at an* angle relative to the flow, a well-documented system of vortices *forms* beneath the hull. Energy is absorbed from this system and *subsequently* increases *its* resistance. *The* vorticity *shed underneath the hull is advected downstream and* interacts with the propeller*. This* is expected to have an negative *effect* on the propulsion efficiency.

Energy Saving Devices (ESDs) have been known to improve performance of vessels in straight ahead conditions by modifying the flow at the aft part of the vessel. The present report considered also the effect of ESDs in drift conditions. Although, the ESD had a neutral effect in resistance significant deterioration of the flow at the propeller plane was observed. The *misalignment* of the ESD axis with the flow seems to have a negative on the overall propulsion efficiency.

In order to mitigate the drift effects on resistance, an optimization study has been carried out on possible hull retrofits in the fore- and aftbody region. The results indicate that a hull shape designed for straight-line operation at a given speed can hold significant optimization potential for use with WAPS. Further, it indicates that a usual optimization for minimum resistance may not provide the definitive answer for operation with WAPS but a focus on added resistance due to side force generation in advisable.

The results on the hydrodynamic behaviour of ships in drift and hell angles, presented in this report will be transferred to WP1 which is responsible for the development of the DSS. These results will be used to describe the hydrodynamic performance of vessels equipped with a wind propulsor.

## References

[1] Renzsch, H., Thies, F., Hydrodynamic Optimization of Ships with Retrofitted WASP-Systems. Proceedings International Conference on Innovation in High Performance Sailing Yachts, 6th Edition, Lorient, FR, 2023.

[2] Renzsch, H., Meyer, J. and Graf, K., Investigation of modern sailing yachts using a new free-surface RANS-code. Proceedings International Conference on Innovation in High Performance Sailing Yachts, 4th Edition, Lorient, FR, 2017.

[3] B. M. Adams, W. J. Bohnhoff, K. R. Dalbey, M. S. Ebeida, J. P. Eddy, M. S. Eldred, R. W. Hooper, P. D. Hough, K. T. Hu, J. D. Jakeman, M. Khalil, K. A. Maupin, J. A. Monschke, E. E. Prudencio, E. M. Ridgway, P. Robbe, A. A. Rushdi, D. T. Seidl, J. A. Stephens, L. P. Swiler, and J. G. Winokur. Dakota 6.21.0 documentation. Technical Report SAND2024-15492O, Sandia National Laboratories, Albuquerque, NM, November 2024. Available online from http://snl-dakota.github.io

[4] Longo, J., and Stern, F. Effects of drift angle on model ship flow. Experiments in Fluids, 32(5), 558–569. https://doi.org/10.1007/s00348-001-0397-0, 2002.

[5] Qiang, Z., Towing tank model test report for a 82000dwt bulk carrier with PSV and HVAF, Model Test Report, CSSRC,2014.

[6] Van, S.H., Kim, W.J., Yim, D.H., Kim, G.T., Lee, C.J., and Eom, J.Y., Flow Measurement Around a 300K VLCC Model, Proceedings of the Annual Spring Meeting, SNAK, Ulsan, ROK, 1998.

[7] Van, S.H., Kim, W.J., Yim, G.T., Kim, D.H., and Lee, C.J., Experimental Investigation of the Flow Characteristics Around Practical Hull Forms, Proceedings 3rd Osaka Colloquium on Advanced CFD Applications to Ship Flow and Hull Form Design, Osaka, Japan, 1998.

[8] Tillig, F., Ringsberg JW. (2020). Design, operation and analysis of wind-assisted cargo ships. Ocean Engineering, Volume 211, DOI: 10.1016/j.oceaneng.2020.107603

[9] Thies, F.; Ringsberg, J.W. (2023). Retrofitting WASP to a RoPax Vessel—Design, Performance and Uncertainties. Energies 2023, 16, 673. https://doi.org/10.3390/en16020673

[10] WASP (2023). WP3 Technical report, EU Interreg project “WASP”, to be published..

[11] Harries, S. and Uharek, S., Application of Radial Basis Functions for Partially-Parametric Modeling and Principal Component Analysis for Faster Hydrodynamic Optimization of a Catamaran, Journal of Marine Science and Engineering, 9(10), 1069, https://doi.org/10.3390/jmse9101069, 2021